Journal of Fluids and Structures (1998) **12,** 259–294

AN EXPERIMENTAL STUDY ON THE FLUIDELASTIC FORCES FOR TWO STAGGERED CIRCULAR CYLINDERS IN CROSS-FLOW

D. S.-K. Ting, D. J. Wang, S. J. Price and M. P. Païdoussis

Department of Mechanical Engineering, McGill University
Montreal, Québec, Canada H3A 2K6

(Received 13 March 1997 and in revised form 1 December 1997)

Both pressure distribution and force measurement techniques have been employed to measure the fluidelastic forces on one of two staggered circular cylinders, of equal diameter, in air cross-flow, for 10 different geometrical arrangements. One cylinder is forced to oscillate transversely to the flow, while the other cylinder remains stationary, and measurements are made either on the oscillating or the stationary cylinder. The forcing frequency, f, is varied from 1 to 16 Hz, with a fixed half peak-to-peak amplitude of 0·043, 0·047 or 0·17 D; the cylinder diameter, D, is fixed at 48·7 mm (1·9 in) and 114·3 mm (4·5 in), respectively, for the force- and pressure-based experiments. The free-stream velocity, U, is varied from 10 to 35 m/s, and this leads to $4 \times 10^4 \leq \mathrm{Re} \leq 2 \times 10^5$ and $15 \leq U/fD \leq 300$. Pressure- and force-based measurements are post-processed in the time and frequency domains, respectively. The amount of hysteresis in the dynamic force coefficients versus cylinder displacement plots increases significantly with decreasing U/fD. The corresponding magnitudes and phase angles of the fluidelastic forces depart rapidly from the asymptotic values when U/fD is reduced below a critical value. This critical value of U/fD is very sensitive to the geometrical arrangement of the two cylinders: it is large when the cylinder is in a sensitive region (where there are rapid changes in static force coefficient with cylinder displacement), and it is much smaller away from these regions.

© 1998 Academic Press Limited

1. INTRODUCTION

Cylindrical structures exposed to fluid cross-flow are found in many practical applications; for example, tube banks in heat exchangers, power transmission lines, marine risers, chimneys and space shuttles subject to atmospheric cross-winds. These structures are subject to flow-induced vibration due to fluid–structure interactions, and possibly even to static or dynamic instabilities. Numerous failures of many practical applications of cylindrical structures subject to fluid cross-flow have been reviewed by Blevins (1977, 1990), Païdoussis (1980, 1981, 1983, 1993) and Chen (1987*a*, *b*). The cost associated with a typical practical failure can easily be of the order of a million dollars. Thus, it is not surprising that extensive effort has been, and still is, focused on the study of such flow-induced vibrations.

A great deal of work has been concerned with the excitation mechanisms associated with flow-induced vibration of cylindrical structures subjected to cross-flow in the last three decades. It is generally agreed that the three principal excitation mechanisms of flow-induced vibration are turbulent buffeting, vortex shedding and fluidelastic instability (Païdoussis 1981). The self-excited fluidelastic instability is potentially the most catastrophic.

0889-9746/98/030259 + 36 $25.00/fl970140 © 1998 Academic Press Limited

1.1. Fluidelastic Forces on Cylinders in Cross-Flow

One way to better understand the fluidelastic behaviour of cylindrical structures subjected to cross-flow is to measure the fluidelastic forces on them. The fluidelastic force in this paper is defined as the dynamic component of the fluid force exerted on a structure, due to either its own motion or the motion of a nearby structure. Generally speaking, measurement of a fluidelastic force with reasonable accuracy is difficult. One reason for this is that the "raw" data from measurements include other fluid dynamic forces, namely those due to turbulent buffeting and periodicity in the flow. In addition, in the case of force measurements on an oscillating cylinder, the fluidelastic force is combined with the inertia force, and extracting the fluidelastic force, which may be smaller than the inertia force, is difficult. It is also noted that because of obvious advantages, fluidelastic force measurements are often conducted in wind tunnels, rather than in water. However, the fluidelastic force in air is much smaller than that in water, since the density of air is about 10^3 lower than that of water. Consequently, it is more difficult to obtain the fluidelastic force with reasonable accuracy in air-flow than in water-flow. It is also important to note that complete information for a fluidelastic force requires both magnitude and phase or, alternatively, both real and imaginary components.

Considering the foregoing, it is not surprising that there is still a lack of sound fluidelastic data in the literature. Nonetheless, complete information on the fluidelastic force has been presented by Otsuki *et al.* (1974), Sarpkaya (1978), Tanaka & Takahara (1980, 1981), Goyder & Teh (1984), Bearman & Luo (1988), Luo & Bearman (1990), and Chen *et al.* (1994), among others; earlier work by Bishop & Hassan (1964) and Tanida *et al.* (1973) should also be mentioned. In general, these studies involve either forced oscillation or free vibration of a flexibly mounted solitary cylinder [e.g., Otsuki *et al.* (1974), Goyder & Teh (1984), Bearman & Luo (1988), and Luo & Bearman (1990)], one or more cylinders in a tube row (Chen *et al.* 1994), or one or more cylinders in a tube array (Tanaka & Takahara 1980, 1981).

1.2. Scope of this Study

This study presents a series of pressure and force measurement results on two staggered circular cylinders of equal diameter subjected to air cross-flow. One of the cylinders is forced to oscillate transversely to the flow direction, while the dynamic forces are measured on either the same or the stationary cylinder. There are two main reasons for investigating the presumably simpler case of two staggered cylinders, instead of studying tube arrays, for example. First, the twin-cylinder system is a representative geometry, actually or as an elemental component in more complex geometries, of practical situations such as in transmission lines, heat exchangers and marine risers. Second, the flow characteristics for the twin-cylinder case are fairly well understood, at least in the static situation. The fluidelastic forces which are present in a tube array exposed to cross-flow depend, among other parameters, on the flow characteristics, which are predominantly determined by the geometrical arrangement of the array. The objective here is to search for possible relationships between the flow characteristics for two staggered cylinders when they are stationary, and the fluidelastic forces acting on them when one of them is forced to oscillate transversely with a small amplitude ($A/D < 0{\cdot}2$). It should be noted here that, particularly in sensitive geometrical arrangements (to be defined and explored later), the fluidelastic forces may be nonlinearly related to A/D; hence, in general, the results with one particular A/D are not easily compared to those with another.

The aim of this study is to examine how the fluidelastic forces (in terms of magnitude and phase angle, or the force coefficient-cylinder displacement path) vary with the reduced flow velocity (U/fD) for different geometrical arrangements of two circular cylinders. Part of this work has been documented in graduate theses (Pinnell 1987; Sychterz 1990; Wang 1995), and has been presented in conferences by Price *et al.* (1988) and Païdoussis *et al.* (1994). This is the first archival publication of part of that work, as well as newer work. In particular, this paper focuses on the experimental techniques, procedures, data analysis methods and presentation of the experimental results. The fluidelastic results presented here can be used to test the validity of models used for predicting the fluidelastic forces on cylindrical structures in cross-flow, e.g. in Ting *et al.* (1997), where the applicability of the quasi-static and quasi-steady assumptions are tested for these configurations.

In general, as a cylinder is displaced statically in the transverse direction, the fluid forces on it and on the other cylinder change. If the cylinder is forced to oscillate over the same transverse path at a given frequency, the fluid forces at any given position differ from the static values, so that, if one plots the total dynamic drag or lift force versus displacement, one generally obtains a hysteresis loop, dependent on geometry and frequency. Furthermore, the fluidelastic components of the force coefficients are not equal to the slope obtained from the curve of the static coefficients versus displacement. If, however, the forcing frequency of oscillation tends to zero, the dynamic force coefficients approach the static values of the appropriate force coefficient slopes, and the hysteresis in the dynamic force versus cylinder displacement plots should vanish.

2. STEADY FLOW PAST TWO STAGGERED CIRCULAR CYLINDERS

The flow field around a pair of stationary cylinders in cross-flow is very complex and has been studied extensively. Interference between two cylinders will occur when they are sufficiently close to each other, or when the downstream cylinder is adjacent to or within the wake of the upstream one. The three types of flow interference suggested by Zdravkovich (1987) are (i) wake interference, (ii) proximity interference, and (iii) combined wake and proximity interference. The boundary separating wake interference from no interference is defined as the line along which the lift coefficient on the downstream cylinder becomes less than 0·01; this boundary is beyond the width of the wake of the upstream cylinder. Proximity interference takes place when the cylinders are close to each other, but neither of them is immersed in the wake of the other. Combined wake and proximity interference represents a combination of (i) and (ii).

A map of the static force coefficients for two circular cylinders of equal diameter subjected to cross-flow in the subcritical Reynolds number regime, as furnished by Zdravkovich (1977, 1987), is regenerated here as Figure 1. Contours of constant static drag and lift coefficients are plotted in the L/D versus T/D plane. (The bold numerical values with arrows designate the 10 different cases considered in this study and will be discussed later.†) Closely packed contours denote regions where small spatial variations in cylinder position can lead to large changes in the static force coefficients. Oscillating the cylinder in these high-gradient regions is expected to result in more complicated fluidelastic characteristics, compared to oscillating it in lower gradient regions. The two sensitive flow regions of particular interest here are the "inner" and "outer" lift peaks, which are centred on the

† Some of the cases studied in this paper are for negative T/D, but for the sake of clarity and because the wake is symmetric about $T/D = 0$, they are shown in Figure 1 for positive T/D.

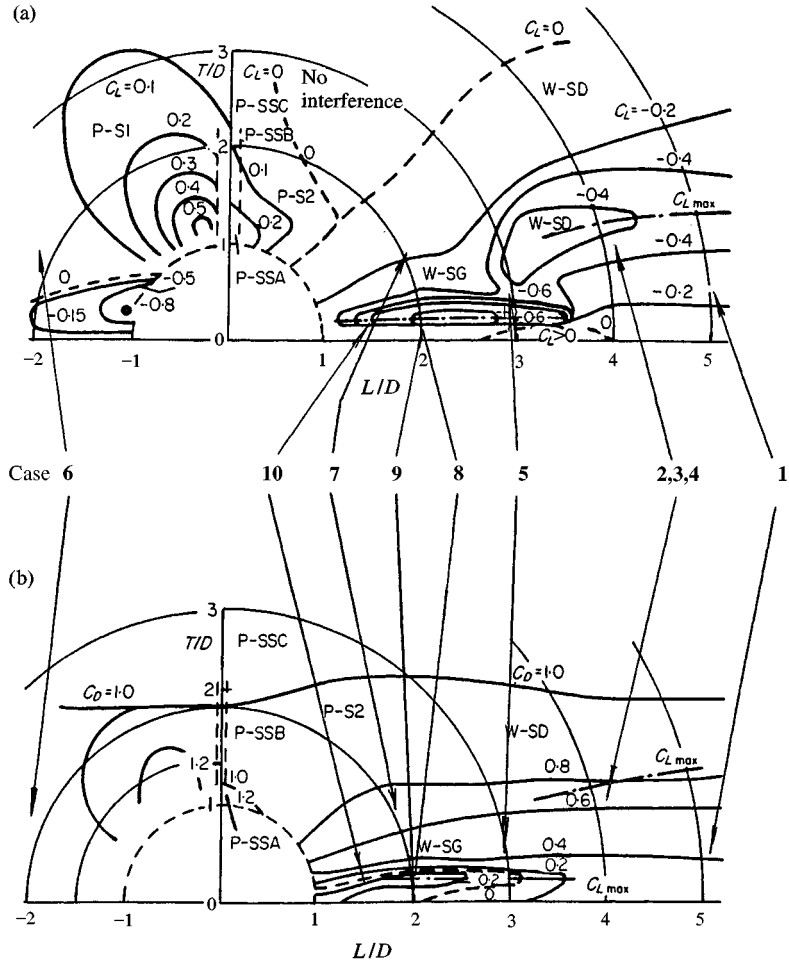

Figure 1. Static force coefficient map for two circular cylinders of equal diameter in cross-flow in the subcritical Reynolds number regime (Zdravkovich 1987): (a) lift coefficient; (b) drag coefficient. Proximity and wake interference regions are designated with the letters "P" and "W", respectively. The corresponding subdivisions of these two interference regions (e.g., the meaning of "P-SSA") and other details are explained in Zdravkovich (1987).

chain-dotted lines marked with $C_{L\max}$ in Figure 1; the inner and outer lift peaks are centred near ($1{\cdot}2 \leq L/D \leq 3{\cdot}5$ and $T/D \simeq 0{\cdot}2$) and ($L/D \geq 4$, $T/D \simeq 1{\cdot}4$), respectively. All of the experimental cases considered in this paper, except one, are either in or around these sensitive flow regions.

The cause for the outer lift peak may be explained in the following three augments. First, for L/D larger than about 3 and T/D larger than 1·4, decreasing T/D by moving the cylinder closer towards the centre-line of the upstream cylinder results in a progressive entrainment of the flow into the wake of the upstream cylinder (Zdravkovich 1977, 1987; Ohya *et al.* 1989). The flow accelerates as it is squeezed into the gap, and this increase in velocity causes a reduction in pressure, and hence, produces a lift on the downstream cylinder directed towards the wake centre-line of the upstream cylinder. Second, the corresponding stagnation point of the downstream cylinder is shifted away from the wake centre-line of the

upstream cylinder (Mair & Maull 1971; Price 1976), indicating a velocity vector pointing downstream and towards the wake centre-line of the upstream cylinder. A resolved component of this drag force in the lift direction gives a lift force acting towards the centre-line of the upstream wake, and may account for about 25% of the total lift force at the outer lift peak (Price 1976). Furthermore, and this is the last of the three arguments, additional circulation produced along the inner side (the side closer to the wake of the upstream cylinder) of the downstream cylinder causes its wake to be deflected outward, away from the wake centre-line of the upstream cylinder, and this also contributes to the total lift force (Price 1976). In short, all three mechanisms contribute to the total lift force, and their relative weight appears to depend on parameters such as L/D and Re. The total lift force peaks at $T/D \simeq 1{\cdot}4$, beyond which it decreases with further reduction in T/D.

The inner lift peak is attributed to the existence and sudden disappearance of the gap flow between the cylinders as T/D decreases. Near the inner lift peak ($1{\cdot}2 \leq L/D \leq 3{\cdot}5$ and $0{\cdot}2 \leq T/D \leq 0{\cdot}5$), the inner side of the downstream cylinder crosses the wake centre-line of the upstream one, and the corresponding flow conditions are such that most of the fluid approaching the downstream cylinder passes through the gap between the two cylinders (Zdravkovich & Pridden 1977; Zdravkovich 1987). Decreasing T/D, by moving the downstream cylinder closer to the wake centre-line of the upstream one, accelerates the gap flow significantly as the flow is squeezed by the two cylinders. This intense gap flow is thought to be responsible for the large lift force directed towards the wake centre-line of the upstream cylinder; the lift force peaks at $T/D \simeq 0{\cdot}2$. With further decrease in T/D, however, the upstream cylinder blocks the gap, and the flow passes around the cylinder pair. This switching from a strong gap flow into one which wraps around the downstream cylinder results in a sudden drop in the lift force as T/D is decreased from 0·20 to around 0·15 (Price & Païdoussis 1984; Zdravkovich 1987).

3. DESCRIPTION OF A FLUIDELASTIC FORCE

The fluidelastic component of a fluid force on a body is motion-dependent (Chen 1987b). It exists only because of the motion of a body and vanishes with cessation of the motion (Parkinson 1989; Price 1995). As previously mentioned, the fluidelastic force can be expressed either in terms of magnitude and phase (Bishop & Hassan 1964; Tanaka & Takahara 1980; Bearman & Luo 1988; Chen 1989), or in terms of real and imaginary parts (Goyder & Teh, 1984; Chen *et al.* 1994). The former of the two is used throughout this paper. A linear fluidelastic force may be decomposed into added mass, fluid damping and fluid stiffness terms. The added mass term is 180° out of phase with the displacement, the fluid damping term is in quadrature (90°) with the displacement and the fluid stiffness term is in phase with it.

In this study, the fluidelastic force coefficients are defined as

$$C_j = \frac{F_j}{\frac{1}{2}\rho U^2 D l}, \tag{1}$$

where $j = 1$ or 2 for drag and lift, respectively, F is the force, ρ is the density of air and l is the length of the cylinder segment in the wind tunnel. They are represented in terms of their magnitude and phase, i.e.

$$C_j = |C_j| \exp[\mathrm{i}(\omega t + \phi_j)], \tag{2}$$

where ϕ_j is the phase angle of C_j with respect to the displacement, $y(t)$.

4. EXPERIMENTAL APPARATUS

The experiments involve two circular cylinders of equal diameter in air cross-flow in a wind tunnel. The forces on one of the cylinders are measured, either indirectly using pressure transducers or directly using force transducers, while forcing either the same cylinder or the other one to oscillate harmonically in the direction transverse to the free stream.

4.1. The Wind Tunnel

The entire series of tests have been conducted in a wind tunnel instead of a water tunnel, mostly due to the difficulty in sealing when oscilating a cylinder in a water tunnel. The wind tunnel used in this study is an open-ended, blow-down tunnel, with a 1·83 m (6 ft) long, 0·91 m (3 ft) wide and 0·62 m (2 ft) high test-section. The free-stream velocity is in the $+X$ direction, which is also the positive drag direction, while positive lift is in the $+Y$ direction; see Figure 2. The wind tunnel is capable of generating steady wind speeds up to 40 m/s when the test-section is empty. During testing, the wind speed is monitored by a Betz manometer, which measures the pressure drop across the contracting section. This was calibrated by measuring the dynamic pressure in the working section with a pitot-static tube. The relationship between the pressure drop in the contracting section and the dynamic pressure in the free stream is linear, with a slope repeatable to within $\pm 5\%$. In the empty test-section, the boundary-layer thickness is less than 18 mm, outside of which the flow velocity variations are less than 0·5%, and the turbulence intensity is less than 0·8%. A more detailed description of the wind tunnel may be found in Pinnell (1987).

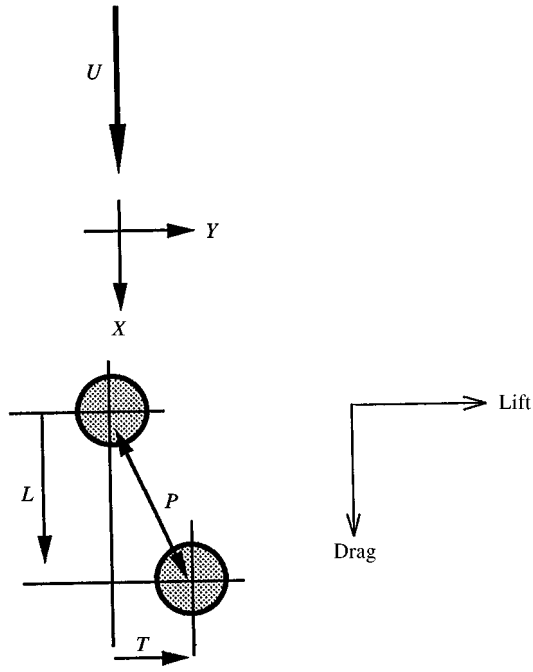

Figure 2. Relative position of the two circular cylinders in cross-flow.

The relative position of the two cylinders is shown in Figure 2. The streamwise and cross-stream distances between cylinders are designated as L and T, respectively, and P is the pitch.

4.2. The Scotch-Yoke Mechanism

One of the most critical parts of the experimental apparatus is the mechanism providing the forced oscillation. This mechanism is required to produce a harmonic oscillation in the transverse direction, of amplitude up to 19·4 mm half peak-to-peak, with minimum distortion, over a frequency range of 1–16 Hz. To achieve this, the oscillating cylinder is mounted via a yoke which fits around the outside of the wind tunnel (Figure 3); on the top and bottom of the wind tunnel, linear bearings are used to guide the yoke and so prevent cylinder motion in the streamwise direction. The yoke is attached to a scotch-yoke mechanism, which provides the required harmonic oscillation; detailed descriptions are given elsewhere (Pinnell 1987; Sychterz 1990; Wang 1995).

4.3. The Cylinder Instrumented With a Pair of Pressure Transducers

The cylinders used in experiments where the forces were determined via pressure measurements are made of seamless (6351-T6) aluminium tubing of 114·3 mm (4·5 in) nominal outside diameter, with a wall thickness of approximately 2 mm. The use of these relatively large diameter cylinders is essential in (i) producing adequate pressure change with angular disposition on the surface, which can be measured with reasonably good accuracy, for relatively small changes in T/D, i.e., small A/D and (ii) in providing enough room for the electronic transducers, amplifier circuits, pressure transducer cables and hoses to be properly mounted inside the cylinder. Consequently, the aspect ratio of the portion of the cylinder in the wind tunnel is low at 5·3, and the blockage ratio is a little high at 12·5%. All results

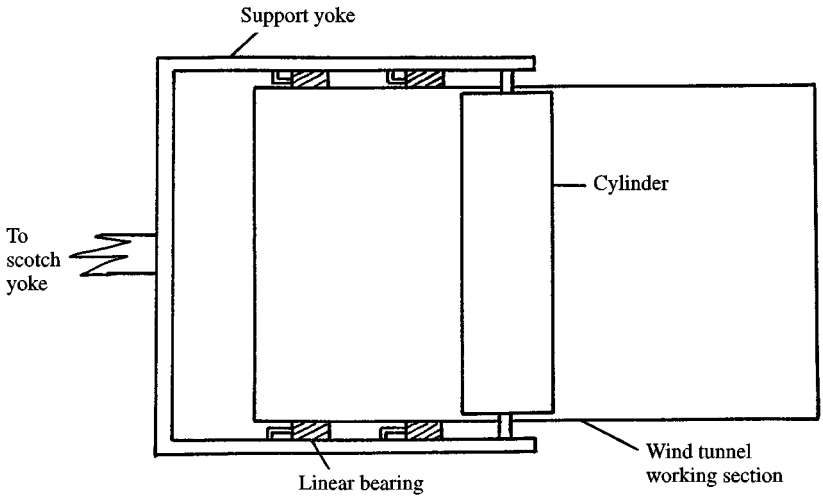

Figure 3. A cross-sectional schematic of the oscillating cylinder in the wind tunnel. The flow is perpendicular to the paper, towards the reader.

presented in this paper are not corrected for blockage since, for the twin-cylinder system with interfering wakes, no well-tested method for such correction is known to the authors.

The pressure transducer used in the pressure measurement experiments is a Celesco variable reluctance pressure transducer; it has a mass of 71 g, and a full-scale pressure range of 50 mm of water (490 N/m^2). Two entirely separate types of calibration procedures have been used to verify the linearity of the pressure transducer. In the first, the two pressure ports of the differential transducer were connected to upstream and downstream locations of the contracting section of the wind tunnel. The transducer was calibrated using a Betz manometer as the standard, over a range of differential pressure levels by adjusting the air speed in the wind tunnel. In the second method, the transducer was connected in parallel to an alcohol-filled inclined manometer and a disposabable "Plasti-Pak" syringe, where the pressure was incremented using the syringe. In both calibrations, the linearity and hysteresis of this transducer are found to be $\pm 0{\cdot}5\%$ full scale, or $\pm 2{\cdot}5$ N/m^2. This suggests that for a maximum error in dynamic pressure of 5%, the minimum flow velocity should be approximately 9 m/s.

In the experiment, one port of the pressure transducer is connected by tubing to a 1·6 mm diameter pressure port, located at the mid-span position of the instrumented cylinder. The second pressure port is connected to a large reservoir mounted inside the cylinder. The reservoir provides a constant pressure source, and all pressure measurements are made relative to this. The effect of this constant pressure source is accounted for by zeroing the transducer output when the pressure port is exposed to static pressure. A dummy transducer with both pressure ports connected to the reservoir is aligned in the same direction as, and next to, the active transducer. This dummy transducer is used to measure the inertial effects. The signal from the active transducer minus that from the dummy transducer gives the "true" dynamic pressure signal. Because the two transducers have very similar sensitivities to temperature, positioning them next to each other and subtracting the signals has the added advantage of providing temperature compensation for the pressure measurements.

4.4. The Cylinder Instrumented With Two Force Transducers

For measurements with force transducers, the cylinder diameter can be considerably smaller than in the foregoing, thereby increasing the aspect ratio of the cylinders and reducing the blockage in the wind tunnel. The diameter of the cylinders in these experiments was reduced from 114·3 to 48·7 mm. The two cylinders are made of capped aluminium tubes of 48·7 mm diameter and 1·5 mm wall thickness. The corresponding aspect ratio of the cylinder segment in the wind tunnel is now 12·8, and the wind tunnel blockage is 5·3%.

Two ISF load cells with ± 15 N range are connected to the two ends of the instrumented cylinder, outside the wind tunnel. For the cases where the instrumented cylinder is also the oscillating cylinder, these force transducers are attached onto the yoke, located outside the wind tunnel test-section. For the cases in which the instrumented cylinder is stationary, these force transducers are supported on the exterior of the upper and lower walls of the wind tunnel. They are positioned such that the force components in both the drag and lift directions can be measured simultaneously. These force transducers are strain-gauge-type sensors which allow both steady and fluctuating force measurements to be made. The calibration of this force measuring system is performed statically using dead weights. Linear load–voltage relationships are obtained from calibrations in both directions, and the maximum repeatability or hysteresis errors in the drag and lift directions are typically 0·1 N (2%) and 0·2 N (3%), respectively.

5. EXPERIMENTAL PROCEDURE AND DATA REDUCTION

The experiments presented in this paper have been conducted in three different series. Pressure-based measurements were used in the first series, where the instrumented cylinder, located downstream of a stationary cylinder, was forced to oscillate transversely to the flow with $A/D = 0{\cdot}17$. In the second series, the oscillating cylinder was instrumented with force transducers, and was forced to oscillate transversely with $A/D = 0{\cdot}047$, again with the other cylinder stationary. In the last series of experiments, the fluidelastic forces on a stationary cylinder, induced by the upstream cylinder oscillating transversely with $A/D = 0{\cdot}043$, were measured using force transducers. The different procedures and data analysis methods used in these three series of experiments are given in the following.

5.1. Pressure-Based Experiments

The fluidelastic forces can be deduced from the pressure distribution along the circumference of the cylinder. Using this procedure, the skin friction contribution is neglected, since over 99% of the drag of bluff bodies in the subcritical Reynolds number regime is due to pressure forces. The advantage of using this procedure is that some aspects of the flow field surrounding the cylinder can be inferred from pressure distribution measurements.

For a reasonably accurate representation of the flow field around the cylinder, pressure must be measured at closely spaced locations around the circumference of the cylinder. Ideally, the pressure distribution should be measured *simultaneously* at all desired locations; however, this would require 36 pressure transducers for an angular resolution of 10°. Evidently, this is not possible due to limited space inside the cylinder, large additional mass to the oscillating cylinder, increased cost and possible flow interference between the pressure tappings. Therefore, only one pressure tapping is employed, and one measurement is made at a time. The cylinder is then rotated in 10° increments, until a complete pressure distribution around the circumference is obtained. Assuming the pressure between adjacent angular positions to vary linearly, the measured pressure distribution is integrated to give the corresponding force coefficients. The major drawback of this method is that a considerable amount of time is required to complete one experiment.

For all pressure-based tests, the cylinder diameter and the half peak-to-peak amplitude are fixed at 114·3 and 19 mm, respectively. For each case, the two cylinders are first aligned so that they are parallel to each other and perpendicular to the horizontal plane of the wind tunnel. The range of forcing frequencies is limited to $1\ \text{Hz} \leq f \leq 6\ \text{Hz}$, due to the relatively large cylinder mass and the maximum force rating of the scotch-yoke meachanism. The corresponding ranges of Reynolds number and reduced flow velocity are $6 \times 10^4 \leq \text{Re} \leq 2 \times 10^5$ and $15 \leq U/fD \leq 250$, respectively.

Prior to the dynamic tests, static pressure measurements are made on stationary staggered cylinders of the same geometrical arrangements as those used in the dynamic tests. The static results are required as inputs to the quasi-steady model, as discussed in Ting *et al.* (1997). The instrumented cylinder is rotated through 10° increments of the circumferential angles read on a large protractor mounted on the upper end of the instrumented cylinder outside the wind tunnel. The pressure at each angular location is measured using a DC voltmeter. The static pressure in the wind tunnel is also simultaneously measured, and thus, the pressure coefficient distribution around the cylinder is obtained. The static force coefficients are obtained by integrating the pressure coefficients around the cylinder circumference. This procedure is repeated with the cylinder statically displaced in seven evenly

spaced steps in the transverse direction, covering the span of the intended oscillation amplitude in the dynamic case, i.e. $\pm A$. Consequently, the variations of static force coefficients with respect to step changes in T/D are obtained.

The experimental procedure is as follows. First, the instrumented, downstream cylinder is forced to oscillate at the desired frequency. This is achieved by adjusting DC-motor speed control until the oscillating frequency, as indicated by an accelerometer mounted inside the oscillating cylinder, has the desired value. Then, for each circumferential position around the cylinder, an ensemble average of the pressure variation with time as the cylinder oscillates is obtained. A triggering device on the scotch-yoke mechanism is used to ensure that each individual signal in the ensemble average is started at exactly the same point in the oscillation cycle. As the pressure measurements are processed in the time domain, the signal contains contributions from all types of fluid dynamic phenomena, including vortex shedding and turbulent buffeting, in addition to the required fluidelastic force. Thus, a large number of synchronized averages (typically 50) is required to filter out these unwanted interfering signals. Having repeated this averaging procedure at 10° increments around the circumference of the cylinder, the pressure signals may be integrated, giving the total (steady plus unsteady) force coefficients, C_D and C_L, as functions of time. In addition, because the cylinder is executing simple harmonic motion, its position may also be calculated as a function of time. Thus, the variations of C_D and C_L with respect to cylinder displacement as the cylinder is oscillated about its mean position are obtained.

5.2. Force-Based Experiments

A more direct way of measuring the fluidelastic forces on the cylinder is achieved when using force transducers. Unlike pressure distribution measurements, force measurements are significantly less time-consuming. However, the less laborious force measurement technique cannot reveal anything on the detailed flow field around the cylinder.

Two different types of force measurement were made: either the forces are measured on the oscillating cylinder while the other cylinder is kept stationary, or they are measured on the stationary cylinder while oscillating the other cylinder.

The cylinders are first aligned, as before. With the oscillating cylinder at its mean position in the lift direction, the relative positions of the two cylinders are measured with an accuracy of $\pm 0{\cdot}5$ mm, thus determining L and T (and also P; see Figure 2) to the same accuracy.

The smaller cylinders used in the series of tests based on force measurements also lead to lower Re, $4 \times 10^4 \leq \mathrm{Re} \leq 1 \times 10^5$. Because of the reduced cylinder mass and improvements made to the design of the scotch-yoke mechanism, the range of forcing frequency is widened to $1\ \mathrm{Hz} \leq f \leq 16\ \mathrm{Hz}$, and the corresponding range of reduced flow velocity is roughly $15 \leq U/fD \leq 300$. The half peak-to-peak amplitude is 2·3 mm for tests in which forces on the oscillating cylinder are measured, and 2·1 mm for tests in which forces on the stationary, downstream cylinder are measured. (The difference in oscillation amplitude is due to small changes made to the scotch-yoke mechanism, i.e., retightening of the screws on the scotch-yoke mechanism two years after completion of the first series of force-measurement tests.)

The measured forces can be processed in the time domain in a similar way to that used for the pressure measurements. However, the procedure can be simplified considerably when the measurements are post-processed in the frequency domain. In the frequency domain, all the fluid dynamic force components are distinguishable. The fluidelastic forces can easily be isolated from the steady and vortex-shedding forces, and the inertia forces, if present, can be

subtracted vectorially. Moreover, the noise interference, which may include both turbulent buffeting and electronic noise, is limited to the component at the forcing frequency only. This noise, which is uncorrelated with the cylinder motion, can be filtered out using an averaging process. Because of these advantages, the force results presented here were analysed in the frequency domain. However, a disadvantage of this method is that the actual path in the force versus displacement plot can only be approximated. This point will become more obvious when we look at the dynamic results is Section 8.

In the frequency domain, the *steady* drag and lift forces are the corresponding DC values at 0 Hz, measured on the instrumented cylinder while the oscillating cylinder is oscillating at the desired frequency. These DC values can be obtained from the power spectra (in frequency domain analysis); they are equal to the mean values in the signal time-traces (in time domain analysis). Similarly, the *static* forces are the mean values in the time domain when both cylinders are stationary, and these static values are equal to the corresponding DC values in the frequency domain. For the force-based experiments, both the static and steady force coefficients are deduced from the mean values in the time domain, and these values are confirmed by the corresponding DC amplitudes at 0 Hz in the frequency spectra.

5.2.1. Measuring dynamic forces on the stationary cylinder

Consider the case where $L/D = 2{\cdot}94$ and $T/D = -0{\cdot}50$ (Case 5; Table 1), with the forces measured on the downstream, stationary cylinder, while oscillating the upstream cylinder in the transverse direction. Typical fluidelastic signals before and after 30 synchronized averages are shown in Figure 4. The forcing frequency is clearly shown in the spectra of the fluidelastic forces. The vortex-shedding frequencies and the structural natural frequencies of the instrumented cylinder and its supporting system, however, are off the scale of the spectra, at much higher frequencies than the forcing frequencies.

In the synchronized averaging process, a specific cylinder motion (for example, when the cylinder crosses the mean position in the lift direction with a positive velocity) is used to trigger the averaging process, giving an ensemble average of segments of time traces starting and ending at the same instants in the cycle of cylinder motion; the corresponding frequency spectra are shown in Figure 4. It is clear from Figure 4 that signals which are uncorrelated with the motion of the oscillating cylinder are reduced significantly, after 30 synchronized averages. A further increase in the number of averages may improve the appearance of the

TABLE 1
A summary of the 10 twin-cylinder cases tested (arranged in decreasing P/D order)

Case	P/D	L/D	T/D	A/D	Vibrating cylinder	Instrumented cylinder	Method of measurement
1	5·02	5·00	0·50	0·17	Downstream	Downstream	Pressure
2	4·13	4·00	1·03	0·047	Downstream	Downstream	Force
3	4·12	4·00	1·00	0·17	Downstream	Downstream	Pressure
4	4·11	3·97	−1·05	0·043	Upstream	Downstream	Force
5	2·98	2·94	−0·50	0·043	Upstream	Downstream	Force
6	2·20	2·00	0·92	0·047	Upstream	Upstream	Force
7	2·06	1·84	−0·93	0·043	Upstream	Downstream	Force
8	2·01	2·00	0·17	0·17	Downstream	Downstream	Pressure
9	2·00	2·00	0·10	0·047	Downstream	Downstream	Force
10	1·51	1·50	0·20	0·17	Downstream	Downstream	Pressure

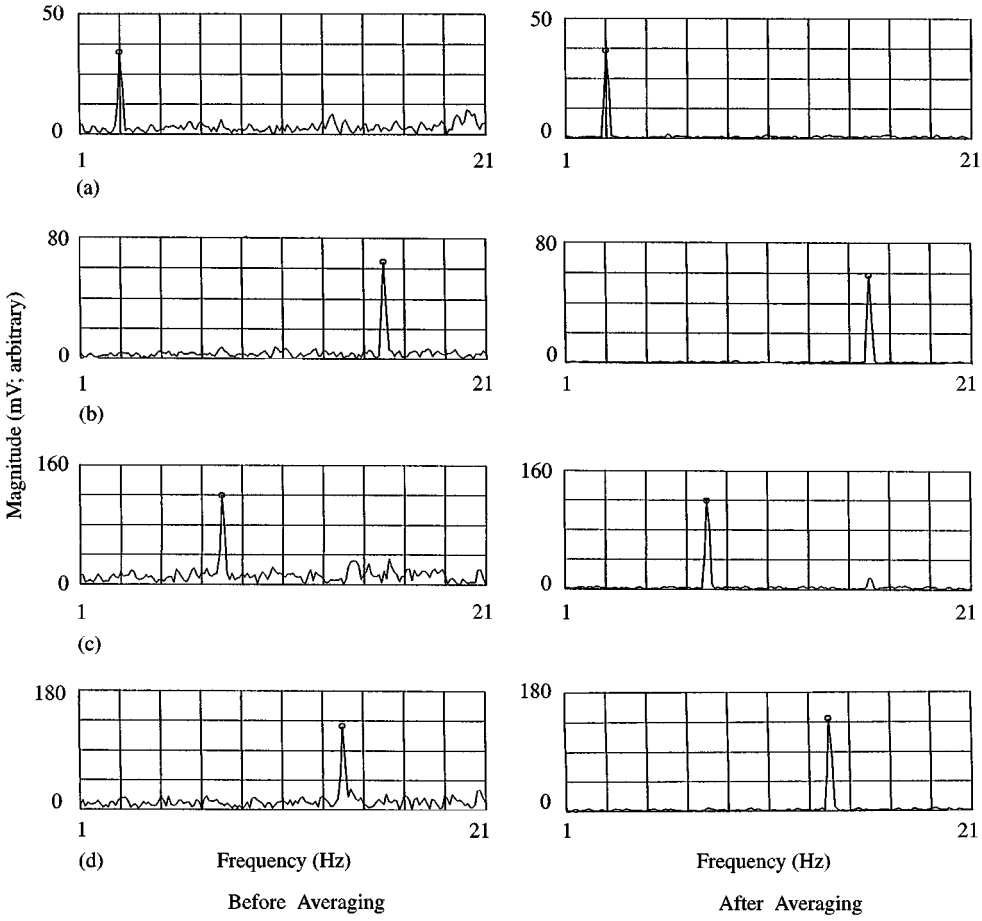

Figure 4. Typical PSDs from force signals before and after 30 synchronized averages: (a) C_D for $f = 3$ Hz; (b) C_D for $f = 16$ Hz; (c) C_L for $f = 8$ Hz; (d) C_L for $f = 14$ Hz.

signal somewhat; however, the magnitude and phase angle of the fluidelastic force do not appear to alter. Thus, the number of averages is fixed at 30 for all cases in which the fluidelastic forces on the stationary cylinder are measured.

5.2.2. Measuring dynamic forces on the oscillating cylinder

When the fluidelastic forces on the oscillating cylinder are required, the procedure is somewhat more complicated. The added mass of the cylinder in the flowing fluid is assumed to be the same as that in the static fluid, and the fluid damping and stiffness forces in still fluid are assumed to be negligible; then, the inertia force due to the mass of the cylinder as well as the added mass can be removed by subtracting vectorially the force signal measured in still fluid from that measured in flowing fluid (Halfman 1952; Fung 1960; Bishop & Hassan 1964; Tanida *et al.* 1973; Washizu *et al.* 1978). The same method is used here, but the subtraction of an inertia force is replaced by a subtraction of mass, which increases the accuracy of the result. If the forces exerted on the cylinder by the fluid are denoted by F_X and

F_Y, and the forces acting on the cylinder by the load cells are R_X and R_Y, the equations of motion of the instrumented cylinder in the drag and lift directions are, respectively,

$$F_X + R_X = k\ddot{y}, \qquad F_Y + R_Y = (m_c + m_a)\ddot{y}, \tag{3}$$

where k is a constant (a small number indicating some coupling of the inertia forces in the lift direction), $\ddot{y}$ is the cylinder acceleration, m_c is the cylinder mass and m_a is the added mass of the cylinder. The corresponding equations in still air, for the oscillating cylinder, are

$$R_{X\mathrm{o}} = k\ddot{y}_\mathrm{o}, \qquad R_{Y\mathrm{o}} = (m_c + m_a)\ddot{y}_\mathrm{o}, \tag{4}$$

where the subscript o denotes that the quantity is measured in still air. It has been assumed in equation (4) that the added mass in still air is the same as that in a flowing air stream, and that the fluid damping and stiffness forces in still air are negligible.

The transfer-function method used by Goyder & Teh (1984) is employed here to obtain the fluidelastic forces. A transfer function is the ratio of output to input, and yields both magnitude and phase as a function of frequency. Taking the transfer function of equations (3) and (4) with respect to $\ddot{y}$ and $\ddot{y}_\mathrm{o}$, respectively, and subtracting one from the other at the forcing frequency yields

$$\frac{F_X}{\ddot{y}} = \frac{R_{X\mathrm{o}}}{\ddot{y}_\mathrm{o}} - \frac{R_X}{\ddot{y}}, \qquad \frac{F_Y}{\ddot{y}} = \frac{R_{Y\mathrm{o}}}{\ddot{y}_\mathrm{o}} - \frac{R_Y}{\ddot{y}}, \tag{5}$$

in which all terms are evaluated at the forcing frequency, f. The same notation as in equations (3) and (4), for the time domain, is used in the frequency domain. The effect of the inertia force has been removed by subtraction of what is effectively a mass, $R_{X\mathrm{o}}/\ddot{y}_\mathrm{o}$ and $R_{Y\mathrm{o}}/\ddot{y}_\mathrm{o}$. Since the cylinder accelerations in the wind-on and wind-off experiments, $\ddot{y}$ and $\ddot{y}_\mathrm{o}$, may not be exactly equal, while m_c, m_a and k are more likely to be the same in the wind-on and wind-off experiments, a subtraction in terms of mass is more accurate than that in terms of inertia force.

A sufficient number of averages is used in the transfer function operations outlined above to eliminate signals which are uncorrelated with the motion of the cylinder (e.g. due to turbulence buffeting).

6. ERROR ANALYSIS

Suppose that a set of primary measurements is made and these measurements are then used to calculate some desired result. The error in the result can be defined as the root-mean square of the errors induced by all the primary measurements. If the result R can be expressed as a function of the primary measurements $a_1, a_2, \ldots, a_n$, that is, $R = R(a_1, a_2, \ldots, a_n)$, then, the error in the result, e_R, is given as (Holman & Gajda 1989)

$$e_R = \left[\left(\frac{\partial R}{\partial a_1}e_1\right)^2 + \left(\frac{\partial R}{\partial a_2}e_2\right)^2 + \cdots + \left(\frac{\partial R}{\partial a_n}e_n\right)^2\right]^{1/2}, \tag{6}$$

where $e_1, e_2, \ldots, e_n$ are the errors of the primary measurements.

A typical error analysis is performed on the steady drag coefficient, $\bar{C}_D$, based on force measurements, keeping in mind that the same evaluation can be performed on $\bar{C}_L$ and the static force coefficients, Again, consider Case 5 ($L/D = 2{\cdot}94$, $T/D = -0{\cdot}50$; Table 1) in which forces on the downstream stationary cylinder are measured, while oscillating the upstream cylinder in the transverse direction. The steady drag coefficient,

$\bar{C}_D = (\bar{F}_D - \bar{F}_{D0})/qDl$, where $\bar{F}_D$ is the mean or steady force in the drag direction with the wind on, $\bar{F}_{D0}$ is the corresponding zero value with the wind off, and q is the dynamic pressure. Then, according to equation (6), the relative error of $\bar{C}_D$ can be expressed as

$$\frac{\Delta \bar{C}_D}{\bar{C}_D} = \left[\left(\frac{\Delta \bar{F}_D}{\bar{F}_D} \right)^2 + \left(\frac{\Delta \bar{F}_{D0}}{\bar{F}_{D0}} \right)^2 + \left(\frac{\Delta q}{q} \right)^2 + \left(\frac{\Delta D}{D} \right)^2 + \left(\frac{\Delta l}{l} \right)^2 \right]^{1/2}. \tag{7}$$

For a typical test at $\mathrm{Re} = 7 \times 10^4$, the values for $\Delta \bar{F}_D/\bar{F}_D$, $\Delta \bar{F}_{D0}/\bar{F}_{D0}$, $\Delta q/q$, $\Delta D/D$ and $\Delta l/l$ are approximately 0·04, 0·05, 0·03, 0·002 and 0·06, respectively. Thus, the relative error of $\bar{C}_D$ is roughly 9%. The relative error of $\bar{C}_L$ is slightly higher at about 10%, due to larger errors in the terms, $\Delta \bar{F}_L/\bar{F}_L$, $\Delta \bar{F}_{L0}/\bar{F}_{L0}$. As the relative position of the two cylinders is measured to an accuracy of $\pm 0{\cdot}5$ mm, the associated errors in the force coefficients are generally small. However, since the instrumented cylinder in Case 5 (and also Cases 8–10) is in a sensitive regime, where small spatial variations can lead to large changes in the force coefficients (see Figure 1), small uncertainties in L and T can increase the total relative error somewhat. Estimating from the static force coefficient versus cylinder position plots, the variations in the static force coefficients with respect to $\pm 0{\cdot}5$ mm changes, in the cylinder position result in an additional 2% relative error, increasing the total relative errors in $\bar{C}_D$ and $\bar{C}_L$ to about 11 and 12%, respectively. Similar calculations can be performed on other cases including the static cases based on pressure distribution measurements. In general, the total errors in the static (for both pressure- and force-based cases) and steady (for force-based cases) force coefficients are less than 12%.

The error analysis for the dynamic coefficients for the force-based cases and the total force coefficients for the pressure-based cases may appear to be more complicated than that for the static and/or steady coefficients, but in fact it is similar. As the fluidelastic forces are caused by cylinder motion, their accuracy depends on f and A, in addition to the other parameters given in equation (7). Let us consider the magnitude of the fluidelastic drag coefficient, $|\tilde{C}_D|$, for Case 5 ($L/D = 2{\cdot}94$, $T/D = -0{\cdot}50$). The relative error of $|\tilde{C}_D|$ may be expressed as

$$\frac{\Delta |\tilde{C}_D|}{|\tilde{C}_D|} = \left[\left(\frac{\Delta \tilde{F}_D}{\tilde{F}_D} \right)^2 + \left(\frac{\Delta \tilde{F}_{D0}}{\tilde{F}_{D0}} \right)^2 + \left(\frac{\Delta f}{f} \right)^2 + \left(\frac{\Delta A}{A} \right)^2 + \left(\frac{\Delta q}{q} \right)^2 + \left(\frac{\Delta D}{D} \right)^2 + \left(\frac{\Delta l}{l} \right)^2 \right]^{1/2}, \tag{8}$$

where $\tilde{F}_D$ is the magnitude of the fluidelastic force in the drag direction with the wind on and $\tilde{F}_{D0}$ is the corresponding zero value with the wind off. In the frequency domain, $\tilde{F}_{D0}$ is zero. For a typical test at $\mathrm{Re} = 7 \times 10^4$ and $f = 8$ Hz, the relative errors for the terms on the right-hand side are estimated to be roughly 0·15, 0, 0·02, 0·01, 0·03, 0·002 and 0·06, respectively. Therefore, for this particular situation, the relative error in $|\tilde{C}_D|$ is roughly 17%. For the same condition, the relative error in $|\tilde{C}_L|$ is somewhat less at about 13%, mostly because $\tilde{F}_L$ is significantly larger than $\tilde{F}_D$. In general, it is probably correct to say that, conservatively, the measured values for the dynamic force coefficient magnitudes, $|\tilde{C}_D|$ and $|\tilde{C}_L|$, for the force-based cases, and the total force coefficients, C_D and C_L, for the pressure-based cases are reliable to within ± 20%. From repeatability tests, the absolute errors in the measured phase angles, ϕ_D and ϕ_L, are found to be less than 15°.

7. STATIC MEASUREMENTS

In this section, the preliminary static test results on a single stationary cylinder are discussed first, followed by the static results for the stationary staggered cylinders.

7.1. A Single Stationary Cylinder

The main reason for performing static tests on a single stationary cylinder is to compare the results obtained here with those in the open literature. This comparison indicates how the wind tunnel flow and the test model used in this study compares with those of other experimenters, so giving an indication of the validity of the whole set of experimental results obtained.

Pressure distributions around the circumference of the large stationary cylinder ($D = 114{\cdot}3$ mm) with and without end-plates have been measured for $7 \times 10^4 \leq \mathrm{Re} \leq 2 \times 10^5$. The pressure measurements are repeatable to within $\pm 0{\cdot}07$ in terms of pressure coefficient. The standard deviation of the pressure coefficient peaks at approximately 70–80° and 280–290°; this indicates that boundary-layer separation occurs on both sides of the cylinder at roughly 70–80° from the front stagnation point, which agrees with other studies in the literature (Achenbach 1968; Batham 1973).

The effects of Re, end-plates and blockage have been considered for this single stationary cylinder. The values of static drag coefficient, C_D, without end-plates are about 16% lower than those with end-plates. With end-plates, C_D decreases from 1·14 to 0·98 as Re increases from $6{\cdot}8 \times 10^4$ to $2{\cdot}0 \times 10^5$. These values of static drag coefficient for a single stationary cylinder ($D = 114{\cdot}3$ mm), obtained using the pressure measurement technique, are within the scatter of the values in the literature ($\simeq 1{\cdot}0$–$1{\cdot}3$), though somewhat lower than the well-accepted value of 1·2 in the subcritical Reynolds regime (Fage & Falkner 1931; Shin & Wambsganss 1977). Sealing the air leakage through the small opening between the cylinder and the upper and lower walls of the tunnel can increase the static drag coefficient by roughly 5%. Thus, the wind tunnel was properly sealed for all subsequent tests. Blockage corrections using the formulae from Allen & Vincenti (1944) reduce the static drag coefficient by roughly 11%.

The forgoing static results for the large cylinder indicate that the values of static drag coefficient obtained in this study are somewhat less than the expected value of 1·2, especially if the present results are corrected for blockage. For this cylinder, the wind tunnel blockage of 12·5% appears to be large enough to have a significant effect on the results and to make direct comparison between the present results and others difficult. With a slightly larger aspect ratio of 6 and the same blockage of 12·5%, West & Apelt (1982) found that C_D decreases significantly with increasing Re above $1{\cdot}1 \times 10^5$; the same qualitative trend of decreasing C_D with increasing Re has been obtained here. Furthermore, Batham (1973) found that for $\mathrm{Re} = 1{\cdot}11 \times 10^5$, increasing the free-stream turbulence from 0·5 to 12·9% decreases C_D from 1·17 to 0·41. Also, for $\mathrm{Re} = 1{\cdot}11 \times 10^5$ and a free-stream turbulence of 0·5%, C_D decreases from 1·17 to 0·72 when roughening the cylinder surface using 0·5 mm diameter sand particles (Batham 1973). For a free-stream turbulence of 1·4%, Norberg & Sundén (1987) found that C_D decreases from 1·36 to 0·48 when increasing Re from $1{\cdot}09 \times 10^5$ to $2{\cdot}25 \times 10^5$. In this study, the free-stream turbulence level was less than 0·8% i.e. somewhat higher than the 0·5% for the low-turbulence case used by Batham. No particular care was taken to ensure a smooth cylinder surface in the present study, although the cylinder was not as rough as Batham's rough cylinder. It appears that the combined effect of cylinder roughness, free-stream turbulence and short aspect ratio could have lowered the critical Reynolds number at which transition from subcritical to critical flow occurs to $\mathrm{Re} \leq 7 \times 10^4$ (Roshko 1961), so producing the low values of C_D measured in these experiments.

The static forces on a stationary cylinder of 48·7 mm diameter without end-plates have also been measured. For this more slender cylinder, the aspect ratio is higher (about 13), and

the blockage is lower (about 5%). Without end-plates, the values of static drag coefficient deduced using the force measurement technique are approximately 1·0 for $4 \times 10^4 \leq \mathrm{Re} \leq 1 \times 10^5$. Accounting for the maximum possible error of 11% in C_D, these values are about 9% lower than the ideal value of 1·2. However, it is expected that utilizing proper end-plates would increase the values of C_D, so that they would be in better agreement with the experimental data in the literature.

In conclusion, the static drag values on a stationary cylinder are either reasonable (large aspect ratio cylinders) or the reasons for their divergence from standard values (low aspect ratio cylinders) can reasonably be explained.

7.2. Two Staggered Cylinders

The ten different cases of staggered cylinders considered in this study, arranged in order of decreasing P/D, are summarized in Table 1. Each case is characterized by L/D, T/D, A/D, which cylinder is being oscillated, which cylinder is instrumented and the measurement technique.

The positions of the ten cases considered here are identified in the static force coefficient map generated by Zdravkovich (1987) in Figure 1 (as indicated in Table 1, Cases 4, 5 and 7 are for negative T/D rather than positive T/D as shown in Figure 1). Though this static force coefficient map is presumably applicable for any general case in the subcritical Reynolds number regime, the values in Zdravkovich (1987) are deduced at $\mathrm{Re} = 6{\cdot}1 \times 10^4$.

Typical comparisons between the values of the static force coefficients obtained in this study, and those estimated from Zdravkovich's (1987) map at $\mathrm{Re} = 6{\cdot}1 \times 10^4$ are tabulated in Table 2. (The steady force coefficient results in Table 2 will be discussed in the next section.) Note that the discrepancy in Re, and more importantly, uncertainties in interpolation for the force coefficients corresponding to any given L/D and T/D can lead to rather significant variations in C_D and C_L. The somewhat larger discrepancies which are associated with the pressure results are probably due to the small aspect ratio in the pressure-measurement results. In general, the values for static force coefficients obtained in this study are in fair agreement with those in Zdravkovich (1987).

8. DYNAMIC MEASUREMENTS AND DISCUSSION

Prior to presenting the fluidelastic results, the time-averaged steady force coefficient results are discussed first. At the end of this section, an attempt is made to arrange all the cases tested in a logical order.

8.1. Time-Averaged Steady Force Coefficients

It is known that when a solitary cylinder is oscillating with a reasonably large amplitude at a high frequency, the steady time-averaged drag coefficient, $\bar{C}_D$, can increase substantially as a result of vortex-excited oscillations (Griffin 1980; Chen 1987*a*, p. 258), associated with widening of the wake. The ratio of steady drag coefficient to static drag coefficient has been found by Griffin (1980) to increase roughly linearly with increasing response parameter, W_r, for $1 \leq W_r \leq 3$, where

$$W_r = \left(1 + \frac{2A}{D}\right)\left(\frac{fD}{US}\right) \tag{9}$$

TABLE 2

Comparisons between the static force coefficients from Zdravkovich (1987, denoted by 'Zdrav') at $\mathrm{Re} = 6{\cdot}1 \times 10^4$, and the static ($C_{Do}$, C_{Lo}) and time-averaged steady force coefficients ($\bar{C}_D$, $\bar{C}_L$) from the present study

Case	L/D	T/D	$\mathrm{Re} \times 10^{-4}$ (present)	C_{Do} (present)	C_{Lo} (present)	C_D† (Zdrav)	C_L† (Zdrav)	$\bar{C}_D$ (present)	$\bar{C}_L$ (present)
1	5·00	0·50	11·6	0·35	−0·05	0·4	−0·2	0·27‡ for $U/fD = 44$	−0·07‡ for $U/fD = 44$
2	4·00	1·03	7·3	0·73	−0·43	0·7	−0·4	$\simeq$ 0·67 for $25 \leq U/fD \leq 140$	$\simeq -0{\cdot}38$ for $25 \leq U/fD \leq 140$
3	4·00	1·00	7·6	0·63	−0·43	0·7	−0·4	0·90‡ for $U/fD = 15$	−0·54‡ for $U/fD = 15$
			11·6	0·58	−0·35			0·65‡ for $U/fD = 132$	−0·41 for $U/fD = 132$
4	3·97	−1·05	7·1	0·76	0·57	0·7	0·4	Between 0·74 and 0·76 for $25 \leq U/fD \leq 240$	Between 0·56 and 0·57 for $25 \leq U/fD \leq 240$
5	2·94	−0·50	7·1	0·21	0·60	0·4	0·6	Decreases from 0·22 to 0·18 with decreasing U/fD from 240 to 30	Increases from 0·59 to 0·65 with decreasing U/fD from 240 to 30
6	2·00	0·92	7·4	0·95	0·01	1·0	0·0	Between 0·92 and 0·93 for $30 \leq U/fD \leq 160$	$\simeq$ 0·01 for $30 \leq U/fD \leq 160$
7	1·84	−0·93	7·1	0·60	0·17	0·7	0·2	Between 0·59 and 0·62 for $30 \leq U/fD \leq 240$	Between 0·17 and 0·18 for $30 \leq U/fD \leq 240$
8	2·00	0·17	7·6	−0·12	0·01	−0·2	0·0	−0·09‡ for $U/fD = 15$	0·00‡ for $U/fD = 15$
9	2·00	0·10	7·1	−0·11	0·03	−0·1	0·0	Between −0·13 and −0·11 for $30 \leq U/fD \leq 250$	Between 0·00 and 0·03 for $30 \leq U/fD \leq 250$
10	1·50	0·20	6·8	−0·07	0·01	0·0	0·0	−0·06‡ for $U/fD = 16$	−0·03‡ for $U/fD = 16$

† Estimated values from Zdravkovich (1987) at $\mathrm{Re} = 6.1 \times 10^4$.

‡ Estimated from the mean values of the total force coefficients, C_D and C_L, for increasing and decreasing y with $y = 0$.

and S is the Strouhal number. It is important to note that while the steady drag coefficient is roughly equal to the static drag coefficient at $W_r = 1$, the data-points show considerable scatter (i.e., up to $\pm 0{\cdot}4$) for $W_r \geq 1$ and no data-points for $W_r < 1$ are included in Griffin's plot.

The maximum W_r considered in this study is less than 0·5. For this small W_r, $\bar{C}_D$ for a solitary cylinder is not expected to depart significantly from the corresponding static value. Typical comparisons between the static and steady force coefficients for the present twin-cylinder cases are given in Table 2; keeping in mind that for the pressure-based cases (Cases 1, 3, 8 and 10), $A/D = 0{\cdot}17$, and the oscillation amplitude is significantly smaller in the force-based cases; i.e. $A/D = 0{\cdot}047$ for Cases 2, 6 and 9, and $A/D = 0{\cdot}043$ for Cases 4, 5 and 7. In all the force-based cases, except one (Case 5), the steady force coefficients, $\bar{C}_D$ and $\bar{C}_L$, remain invariant with respect to U/fD, over the range of conditions considered. In general, these steady force coefficients are, within experimental error (note that the static and steady tests were usually conducted on different days), equal to the corresponding static values ($C_{D\text{o}}$ and $C_{L\text{o}}$) when the "oscillating" cylinder is stationary at its mean lift position. For these cases, the values of $\bar{C}_D$ and $\bar{C}_L$ are either scattered within a narrow range, or remain approximately constant. For the cases where there are definite changes in $\bar{C}_D$ and $\bar{C}_L$ with respect to U/fD, the trends, as well as the minimum and maximum values, are also given in Table 2.

In Case 5, the steady force coefficients, $\bar{C}_D$ and $\bar{C}_L$, measured on the stationary, downstream cylinder while oscillating the upstream cylinder, deviate from the static values, $C_{D\text{o}}$ and $C_{L\text{o}}$, with increasing forcing frequency. The steady force coefficients, $\bar{C}_D$ and $\bar{C}_L$, for Case 5 at $\text{Re} = 7{\cdot}1 \times 10^4$ are plotted against the reduced flow velocity in Figure 5. Although the deviations in $\bar{C}_D$ and $\bar{C}_L$ from $C_{D\text{o}}$ and $C_{L\text{o}}$, respectively, for U/fD less than roughly 50 are small ($<0{\cdot}1$), the results are consistent (over $5{\cdot}5 \times 10^4 \leq \text{Re} \leq 9{\cdot}5 \times 10^4$): $\bar{C}_D$ becomes progressively smaller than $C_{D\text{o}}$ and $\bar{C}_L$ progressively more positive than $C_{L\text{o}}$ with decreasing

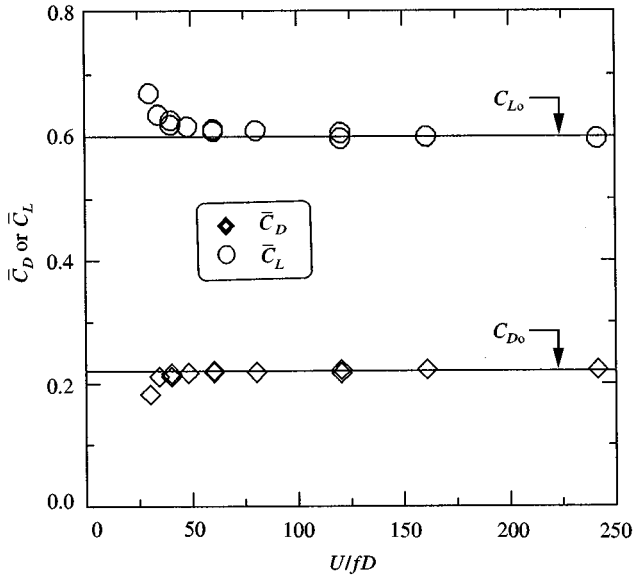

Figure 5. Steady force coefficients, $\bar{C}_D$ and $\bar{C}_L$, for Case 5 ($L/D = 2{\cdot}94$, $T/D = -0{\cdot}50$, $A/D = 0{\cdot}043$) at $\text{Re} = 7{\cdot}1 \times 10^4$ as functions of reduced flow velocity, U/fD. Lines denote the static force coefficients, $C_{D\text{o}}$ and $C_{L\text{o}}$, obtained with the cylinder stationary at its mean position.

U/fD (for $U/fD < 50$). Possibly, the wake of the upstream cylinder may be widened at higher oscillation frequencies; the resulting effect would be to effectively shift this configuration into the inner lift flow conditions, thus decreasing the drag and increasing the lift of the downstream cylinder. However, at the present time the authors have no direct evidence for this hypothesis.

With larger A/D in the pressure-based cases, the effect of U/fD on the steady time-averaged force coefficients is expected to be larger. Unfortunately, the steady time-averaged force coefficients, $\bar{C}_D$ and $\bar{C}_L$, were not measured in the pressure-based cases. The "mean" dynamic force coefficient for the pressure-based cases (cases 1, 3, 8 and 10) in Table 2 are estimated from the curves of total force coefficients as functions of cylinder displacement. The values shown in Table 2 are the mean values of force coefficients when $y = 0$ for increasing and decreasing y. These "mean" dynamic force coefficients are moderately different from the corresponding static values, $C_{D\mathrm{o}}$ and $C_{L\mathrm{o}}$. For the conditions considered, the maximum deviation in the "mean" dynamic force coefficients from the corresponding static coefficients, $C_{D\mathrm{o}}$ and $C_{L\mathrm{o}}$, is less than 0·3. Because these "mean" force coefficients can only be estimates of the true $\bar{C}_D$ and $\bar{C}_L$ in the pressure-based cases, direct comparison between these pressure-based results and the force-based results discussed in the foregoing cannot be made.

8.2. Fluidelastic Force Coefficients

The dynamic results are discussed in an order inspired by the static force coefficient map of Figure 1. Specifically, the discussion of the fluidelastic results is divided into four subsections, corresponding to their (L/D, T/D) location in the map: (i) in the simple wake interference region, (ii) near the outer lift peak, (iii) in and around the inner lift peak, and (iv) in the weak proximity interference region.

8.2.1. Simple wake interference region

In Case 1 ($L/D = 5{\cdot}00$, $T/D = 0{\cdot}50$, $A/D = 0{\cdot}17$, pressure analysis on the oscillating cylinder in the time domain), the instrumented, oscillating cylinder is in the wake of the upstream, stationary cylinder, but is relatively far away from both the inner and outer lift peaks; see Figure 1. Thus, the flow structure is not sensitively dependent on small cylinder displacements. Figure 6 is a plot of the total force coefficients (including both the dynamic and steady components), C_D and C_L, as functions of the normalized cylinder displacement, y/D, for $\mathrm{Re} = 1{\cdot}16 \times 10^5$ and $U/fD = 44$. The figure shows that the total force coefficients do not vary significantly over the range of y/D considered, and the amount of hysteresis is small.

8.2.2. Near outer lift peak

The instrumented cylinder in Case 3 ($L/D = 4{\cdot}00$, $T/D = 1{\cdot}00$, $A/D = 0{\cdot}17$, pressure analysis on the oscillating cylinder in the time domain) is again located in the wake of the upstream stationary cylinder; see Figure 1. In this case, the cylinder oscillates near, but not in, the outer lift peak region. Consequently, the total force coefficients, C_D and C_L, should vary a little more with cylinder displacement compared to those of Case 1 under similar flow conditions, i.e. for the same Re and A/D.

The total force coefficients, C_D and C_L, for Case 3 are plotted as functions of y/D in Figure 7(a) for $\mathrm{Re} = 7{\cdot}55 \times 10^4$ and $U/fD = 15$, and in Figure 7(b) for $\mathrm{Re} = 1{\cdot}16 \times 10^5$ and $U/fD = 132$. The objective in constructing such figures is to study the effect of U/fD; hence, ideally, Re should remain fixed while varying U/fD, thus excluding possible variations in the flow due to change in Re. Unfortunately, the range of forcing frequency is limited by the

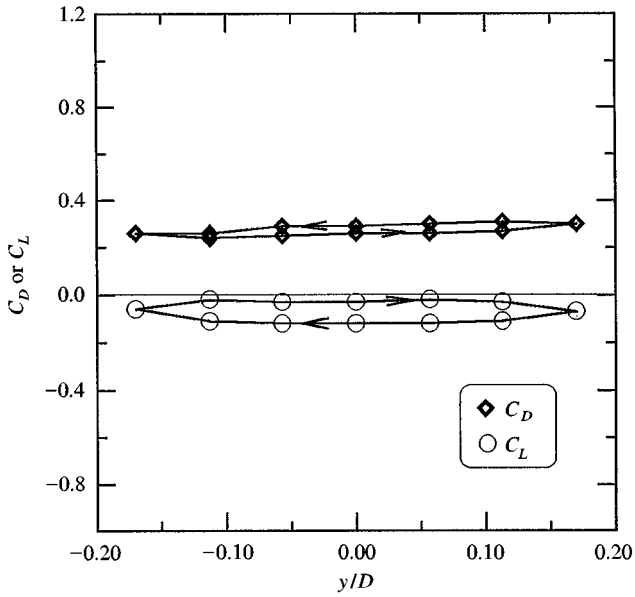

Figure 6. Total (steady plus unsteady) force coefficients, C_D and C_L, on the oscillating, downstream cylinder for Case 1 ($L/D = 5{\cdot}00$, $T/D = 0{\cdot}50$, $A/D = 0{\cdot}17$) at $\mathrm{Re} = 1.16 \times 10^5$ and $U/fD = 44$ as functions of cylinder displacement, y/D.

scotch-yoke mechanism, and is not wide enough to provide the required range of U/fD without altering Re. Nevertheless, both $\mathrm{Re} = 1{\cdot}16 \times 10^5$ and $\mathrm{Re} = 7{\cdot}55 \times 10^4$ should be in the subcritical flow regime[§], and any effects on the dynamic forces caused by the change in Re are expected to be small. Note that for this case, increasing Re from $7{\cdot}55 \times 10^4$ to $1{\cdot}16 \times 10^5$ decreases the magnitudes of $C_{D\mathrm{o}}$ and $C_{L\mathrm{o}}$ by roughly 0·05 and 0·08, respectively; see Table 2. These changes in the static force coefficients are expected to shift the whole C_D and C_L curves up or down by roughly proportional amounts, i.e., without affecting the C_D and C_L versus y/D loops significantly. It is clear when comparing Figure 7(a) to 7(b), that the amount of hysteresis decreases significantly when U/fD is increased from 15 to 132.

As expected, the dynamic force coefficients for Case 3 vary more widely with y/D compared to those for Case 1; for the same Re, compare Figure 7(b) with Figure 6. In addition, the amount of hysteresis in C_D and C_L for Case 3 is significantly larger than for Case 1.

Other than the differences in A/D and the measurement technique used, Case 2 ($L/D = 4{\cdot}00$, $T/D = 1{\cdot}03$, $A/D = 0{\cdot}047$, force analysis on the oscillating cylinder in the frequency domain) is similar to Case 3, that is, the instrumented cylinder in Case 2 is also oscillating in the wake interference region and is close to the outer lift peak. Typical values for the magnitudes of fluidelastic force coefficients, $|\tilde{C}_D|$ and $|\tilde{C}_L|$, and the phase angles of $\tilde{C}_D$ and $\tilde{C}_L$ with respect to $y(t)$, ϕ_D and ϕ_L, are plotted against U/fD in Figure 8(a, b). Although $|\tilde{C}_D|$ appears to increase slightly with increasing Re, the trend is weak; i.e., over the range of conditions considered, Re has no significant effect on the fluidelastic force coefficients. Figure 8 shows that $|\tilde{C}_D|$, $|\tilde{C}_L|$, ϕ_D and ϕ_L remain roughly constant for U/fD

[§] This is not certain, because of the discussion in the fourth paragraph of Section 7.1.

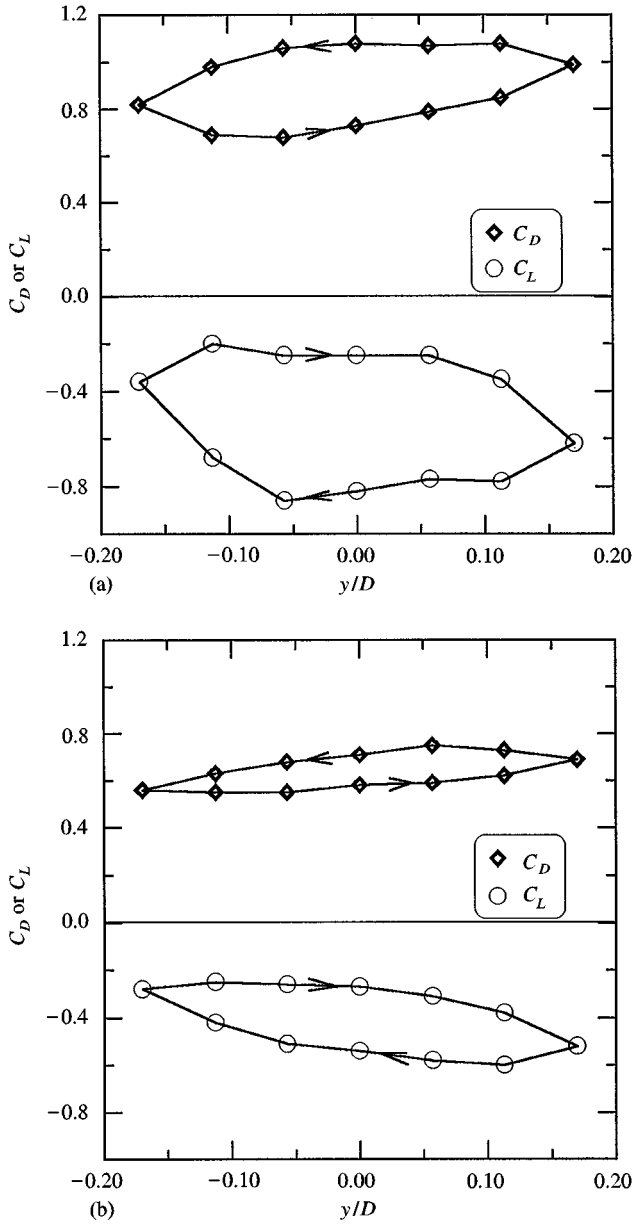

Figure 7. Total (steady plus unsteady) force coefficients, C_D and C_L, on the oscillating, downstream cylinder for Case 3 ($L/D = 4{\cdot}00$, $T/D = 1{\cdot}00$, $A/D = 0{\cdot}17$) as functions of cylinder displacement, y/D: (a) Re $= 7{\cdot}55 \times 10^4$ and $U/fD = 15$; (b) Re $= 1{\cdot}16 \times 10^5$ and $U/fD = 132$.

greater than about 60, tending asymptotically to the constant values shown as horizontal lines. According to the quasi-static assumption, the dynamic values are approximately equal to the quasi-static values (where the phase angle, $\phi = 0$ or $\pm 180^\circ$) for a sufficiently large U/fD. (In the time domain, these quasi-static values are indicated by near-zero hysteresis in the dynamic force versus cylinder displacement plot.)

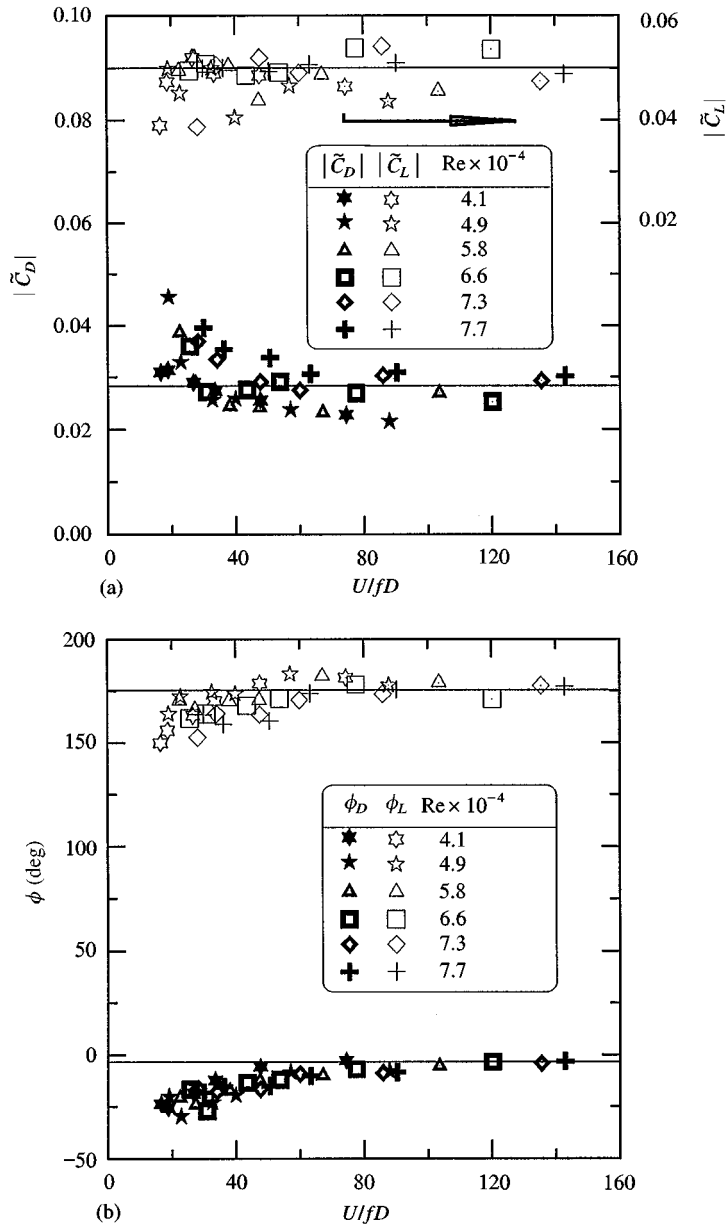

Figure 8. The fluidelastic force coefficients, $\tilde{C}_D$ and $\tilde{C}_L$, on the oscillating, downstream cylinder for Case 2 ($L/D = 4{\cdot}00$, $T/D = 1{\cdot}03$, $A/D = 0{\cdot}047$) as functions of the reduced flow velocity, U/fD: (a) magnitudes, $|\tilde{C}_D|$ and $|\tilde{C}_L|$; (b) phase angles of the fluid forces with respect to the cylinder displacement, ϕ_D and ϕ_L. The horizontal lines denote the asymptotes which are defined as the averages of the three data-points at the largest U/fD.

In order to better compare the results for Cases 2 and 3, typical results from Case 2 with $\mathrm{Re} = 7{\cdot}7 \times 10^4$ in the frequency domain (Figure 8) are converted into C_D and C_L as functions of y/D, in the time domain, and replotted in Figure 9. The conversion is achieved simply by substituting the corresponding values for the magnitude, phase and frequency in

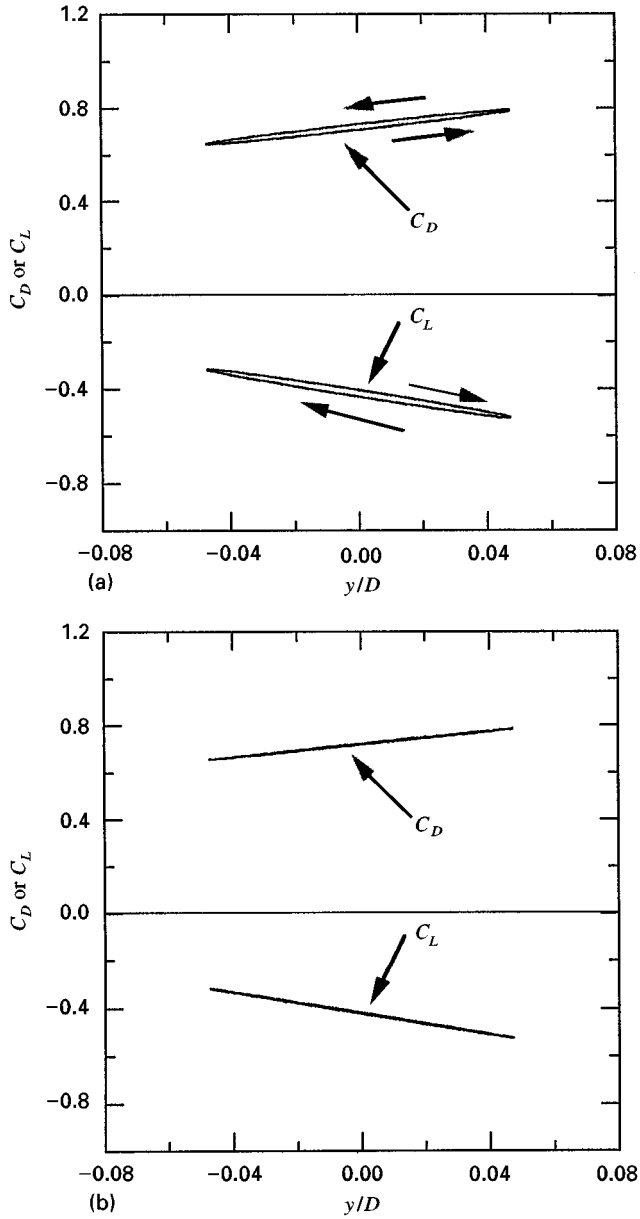

Figure 9. Total (steady plus unsteady) force coefficients, C_D and C_L, on the oscillating, downstream cylinder for Case 2 ($L/D = 4{\cdot}00$, $T/D = 1{\cdot}03$, $A/D = 0{\cdot}047$) at $\mathrm{Re} = 7{\cdot}7 \times 10^4$ as functions of cylinder displacement, y/D: (a) $U/fD = 30$; (b) $U/fD = 143$.

equation (2), and adding the corresponding steady values at each y/D. For Case 2, $\bar{C}_D$ and $\bar{C}_L$ do not vary with changes in the forcing frequency, and hence the steady values at each y value (for $-A \leq y \leq A$) are assumed to be equal to the corresponding static values. The minimum and maximum reduced flow velocities tested ($U/fD = 30$ and 143) at

$\mathrm{Re} = 7{\cdot}7 \times 10^4$ have been used, as they are closest to the two conditions tested in Case 3 ($U/fD = 15$ and $\mathrm{Re} = 7{\cdot}55 \times 10^4$; $U/fD = 132$ and $\mathrm{Re} = 1{\cdot}16 \times 10^5$). The general trends of C_D and C_L as functions of y/D are the same as those in Case 3; compare Figure 9 with Figure 7 [for similar Re, the comparison should be made between Figures 9(a b) and 7(a)]. Similarly to Figure 7, Figure 9 shows that the amount of hysteresis decreases markedly when U/fD is increased from 30 in Figure 9(a) to 143 in Figure 9(b). However, the amount of hysteresis in Case 2 (Figure 9) is significantly smaller than in Case 3 (Figure 7). This discrepancy is believed to be due mostly to the difference in A/D: $A/D = 0{\cdot}047$ for Case 2 and $A/D = 0{\cdot}17$ for Case 3.

Case 4 ($L/D = 3{\cdot}97$, $T/D = -1{\cdot}05$, $A/D = 0{\cdot}043$, force analysis on the stationary cylinder in the frequency domain) is similar to Case 2, but with two major differences: (i) instead of the downstream cylinder, the upstream cylinder is forced to oscillate, while measuring the forces on the downstream, stationary cylinder; and (ii) the oscillation amplitude is about 10% less than that used in Case 2, i.e., $A/D = 0{\cdot}043$ instead of 0·047. The magnitudes of the fluidelastic force coefficients, $|\tilde{C}_D|$ and $|\tilde{C}_L|$, for $\mathrm{Re} = 7{\cdot}1 \times 10^4$ are plotted against U/fD in Figure 10(a), and the corresponding phase angle of $\tilde{C}_D$ for the downstream cylinder with respect to $y(t)$ for the upstream one, ϕ_D, in Figure 10(b). For this case, $|\tilde{C}_L|$ is very small, and this results in large errors in ϕ_L and hence leads to unreliable results; therefore, ϕ_L is not presented here. Figure 10 shows that the values for $|\tilde{C}_D|$, $|\tilde{C}_L|$, and ϕ_D remain roughly constant for U/fD larger than about 60. For U/fD smaller than 60, both $|\tilde{C}_D|$ and ϕ_D deviate rapidly from the corresponding asymptotic values. These results hold true for all values of Re tested. Over the range of Re from 4×10^4 to 1×10^5 considered, the whole $|\tilde{C}_D|$ curve is shifted up by a small amount, and the $|\tilde{C}_L|$ and ϕ_D curves remain roughly unchanged with increasing Re; most importantly, the critical reduced velocity at which $|\tilde{C}_D|$, $|\tilde{C}_L|$ and/or ϕ_D deviate from the corresponding asymptotic values remain fixed at approximately 60.

8.2.3. In and around the inner lift peak

Though of different L/D, both Case 8 ($L/D = 2{\cdot}00$, $T/D = 0{\cdot}17$, $A/D = 0{\cdot}17$, pressure analysis on the oscillating cylinder in the time domain) and Case 10 ($L/D = 1{\cdot}50$, $T/D = 0{\cdot}20$, $A/D = 0{\cdot}17$, pressure analysis on the oscillating cylinder in the time domain) are pressure-based tests in the sensitive flow region close to the inner lift peak; see Figure 1. Consequently, some unusual fluidelastic behaviour is expected from these two cases. The values of the total force coefficients, C_D and C_L, for Cases 8 and 10 are plotted as functions of y/D in Figures 11 and 12, respectively. It is obvious from Figure 11(a) that the fluidelastic characteristics for Case 8 at $U/fD = 15$ are extremely complicated. These complexities are lessened significantly as U/fD is increased to 250, see Figure 11(b). Similarly, for Case 10, Figure 12 shows the complicated paths traced by the force coefficients, C_D and C_L, for $\mathrm{Re} = 6{\cdot}8 \times 10^4$ and $U/fD = 16$.

Similarly to Cases 8 and 10, Case 9 ($L/D = 2{\cdot}00$, $L/D = 0{\cdot}10$, $A/D = 0{\cdot}047$, force analysis on the oscillating cylinder in the frequency domain) is in the area close to the inner lift peak; see Figure 1. The values for the magnitudes of the fluidelastic forces, $|\tilde{C}_D|$ and $|\tilde{C}_L|$, and the corresponding phase angles, ϕ_D and ϕ_L, are plotted as functions of U/fD in Figure 13(a, b). It is clear that the scatter in the data-points in Figure 13 is quite significant. The scatter is due mostly to the complexity of the flow in this sensitive flow region. Nevertheless, the degree of scatter tends to decrease with increasing U/fD; roughly speaking, the results approach asymptotic values for U/fD larger than about 140.

As shown in Figure 1, Case 5 ($L/D = 2{\cdot}94$, $T/D = -0{\cdot}50$, $A/D = 0{\cdot}043$, force analysis on the stationary downstream cylinder in the frequency domain, while oscillating the upstream

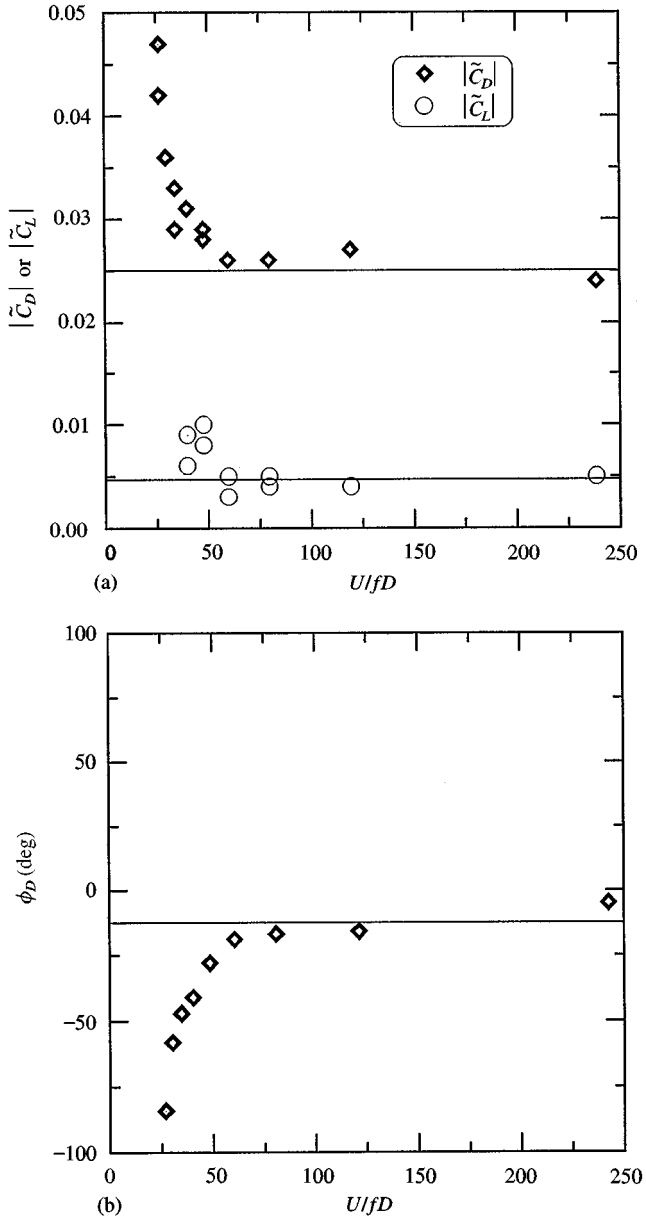

Figure 10. The fluidelastic force coefficients, $\tilde{C}_D$ and $\tilde{C}_L$, on the stationary, downstream cylinder for Case 4 ($L/D = 3{\cdot}97$, $T/D = -1{\cdot}05$, $A/D = 0{\cdot}043$) at Re $= 7{\cdot}1 \times 10^4$ as functions of the reduced flow velocity, U/fD: (a) magnitudes, $|\tilde{C}_D|$ and $|\tilde{C}_L|$; (b) phase angle of the drag on the downstream cylinder with respect to the displacement of the upstream one, ϕ_D. The horizontal lines denote the asymptotes which are defined as the averages of the three data-points at the largest U/fD.

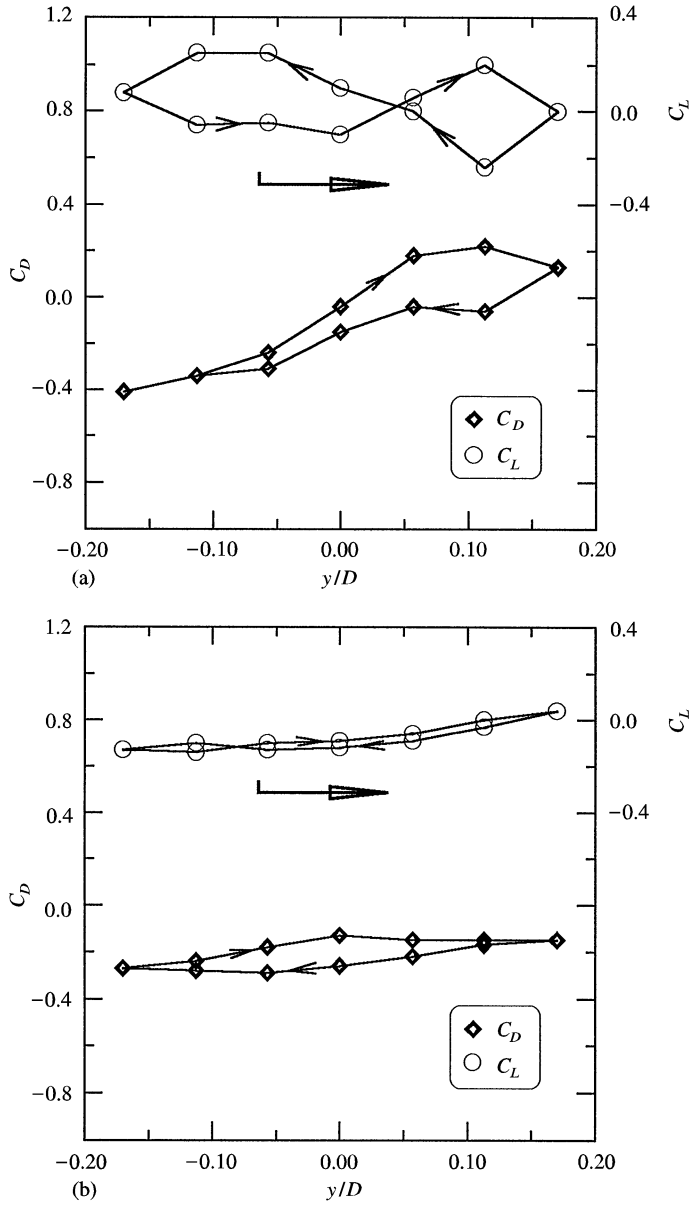

Figure 11. Total (steady plus unsteady) force coefficients, C_D and C_L, on the oscillating, downstream cylinder for Case 8 ($L/D = 2{\cdot}00$, $T/D = 0{\cdot}17$, $A/D = 0{\cdot}17$) as functions of cylinder displacement, y/D: (a) $\mathrm{Re} = 7{\cdot}55 \times 10^4$ and $U/fD = 15$; (b) $\mathrm{Re} = 2{\cdot}16 \times 10^5$ and $U/fD = 250$.

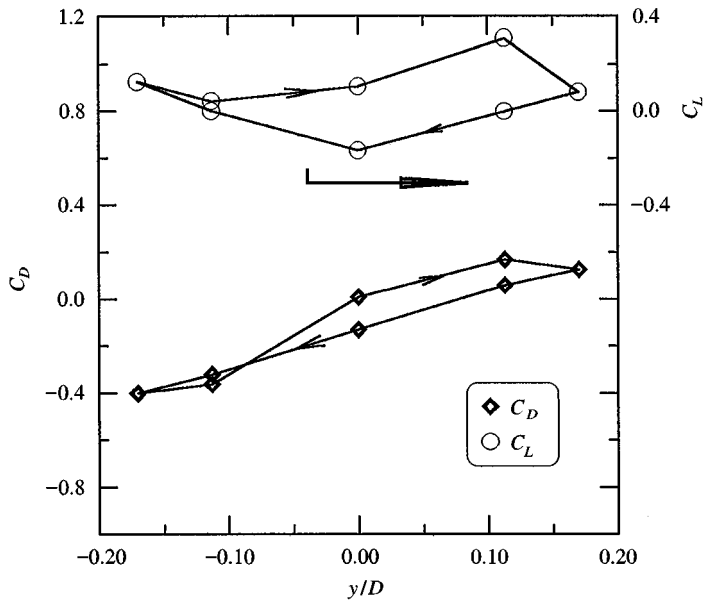

Figure 12. Total (steady plus unsteady) force coefficients, C_D and C_L, on the oscillating, downstream cylinder for Case 10 ($L/D = 1{\cdot}50$, $T/D = 0{\cdot}20$, $A/D = 0{\cdot}17$) at Re $= 6{\cdot}8 \times 10^4$ and $U/fD = 16$ as functions of cylinder displacement, y/D.

cylinder) is on the boundary of the inner lift peak region. Since it is not in the centre of the sensitive flow region, the flow and consequently the fluidelastic characteristics are expected to be less complex than for Cases 8–10, but more so that Cases 1–4 already discussed. The values of $|\tilde{C}_D|$ and $|\tilde{C}_L|$ are plotted as functions of U/fD in Figure 14(a), and the corresponding phase angles of the fluid force on the downstream cylinder with respect to $y(t)$ for the upstream cylinder, ϕ_D and ϕ_L, in Figure 14(b); the particular set of experimental results shown are for Re $= 7{\cdot}1 \times 10^4$, which is in the middle of the Re range tested. The whole set of $|\tilde{C}_L|$ data-points is shifted up slightly, and the $|\tilde{C}_D|$, ϕ_D and ϕ_L curves remain roughly unchanged, with increasing Re from 4×10^4 to 1×10^5. The general trends and the critical U/fD of approximately 125, at which the fluidelastic forces depart from their asymptotic values, remain unaltered over the range of Re considered. Note that the values for $|\tilde{C}_L|$ in Case 5 are much larger than those in Case 4, i.e., roughly 20 times larger! Evidently, the effect of an oscillating upstream cylinder on the lift of a downstream one can be quite large.

While the value of L/D is similar to those of Cases 8 and 9, the instrumented cylinder in Case 7 ($L/D = 1{\cdot}84$, $T/D = -0{\cdot}93$, $A/D = 0{\cdot}043$, force analysis on the stationary cylinder in the frequency domain) is outside and well removed from the inner lift peak region; see Figure 1. The magnitudes of the fluidelastic forces, $|\tilde{C}_D|$ and $|\tilde{C}_L|$, and the corresponding phase angles, ϕ_D and ϕ_L, are plotted as functions of U/fD in Figure 15(a, b), for Re $= 7{\cdot}1 \times 10^4$. It is clear from Figure 15 that these values remain roughly constant for U/fD larger than about 50; this is true for all values of Re tested. For this case, both $|\tilde{C}_D|$ and $|\tilde{C}_L|$ curves are shifted up very slightly with increasing Re.

From the results presented in this section, it is clear that while the fluidelastic characteristics are very complex for cylinder positions around the inner lift peak region (Cases 8–10)

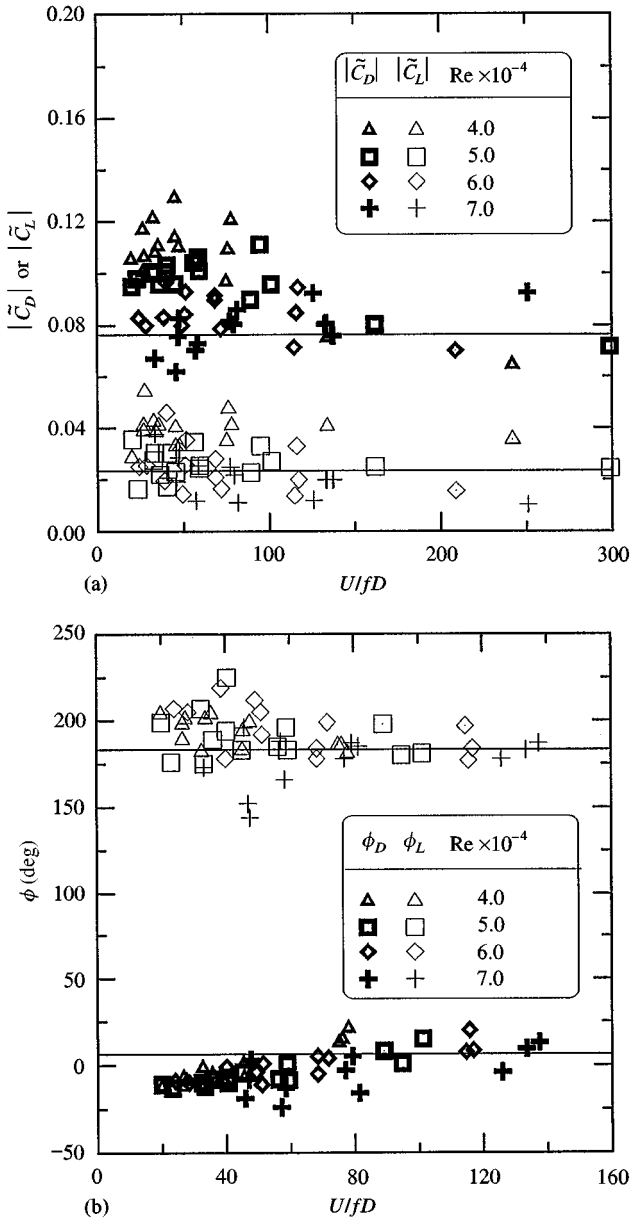

Figure 13. The fluidelastic force coefficients, $\tilde{C}_D$ and $\tilde{C}_L$, on the oscillating, downstream cylinder for Case 9 ($L/D = 2{\cdot}00$, $T/D = 0{\cdot}10$, $A/D = 0{\cdot}047$) as functions of the reduced flow velocity, U/fD: (a) magnitudes, $|\tilde{C}_D|$ and $|\tilde{C}_L|$; (b) phase angles of the fluid forces with respect to the cylinder displacement, ϕ_D and ϕ_L. The horizontal lines denote the asymptotes which are defined as the averages of the three data-points at the largest U/fD.

the complexity is reduced moderately on the boundary of the sensitive region (Case 5); and outside the sensitive flow region (Case 7), the complexity is lessened substantially.

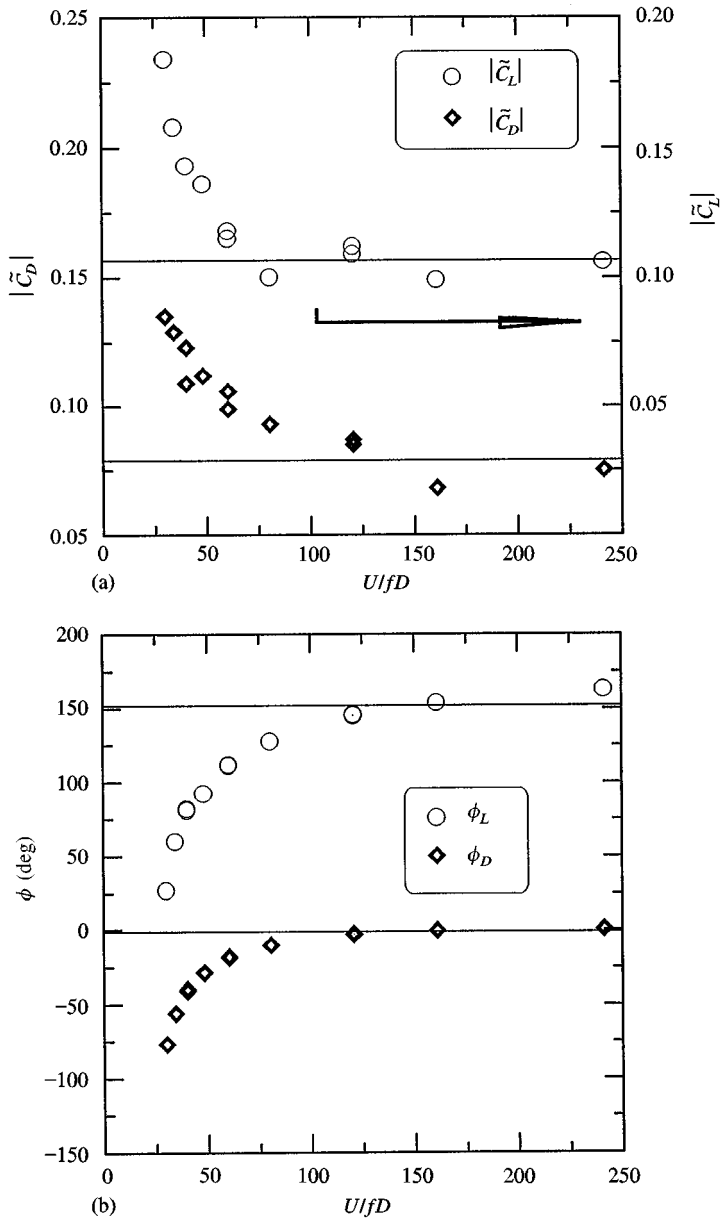

Figure 14. The fluidelastic force coefficients, $\tilde{C}_D$ and $\tilde{C}_L$, on the stationary, downstream cylinder for Case 5 ($L/D = 2{\cdot}94$, $T/D = -0{\cdot}50$, $A/D = 0{\cdot}043$) at $\mathrm{Re} = 7{\cdot}1 \times 10^4$ as functions of the reduced flow velocity, U/fD: (a) magnitudes, $|\tilde{C}_D|$ and $|\tilde{C}_L|$; (b) phase angles of the fluid forces on the downstream cylinder with respect to the displacement of the upstream one, ϕ_D and ϕ_L. The horizontal lines denote the asymptotes which are defined as the averages of the three data points at the largest U/fD.

8.2.4. Weak proximity interference

It can be seen from Figure 1 that Case 6 ($L/D = 2{\cdot}00$, $T/D = 0{\cdot}92$, $A/D = 0{\cdot}047$, force analysis on the oscillating, upstream cylinder in the frequency domain) is the only case in

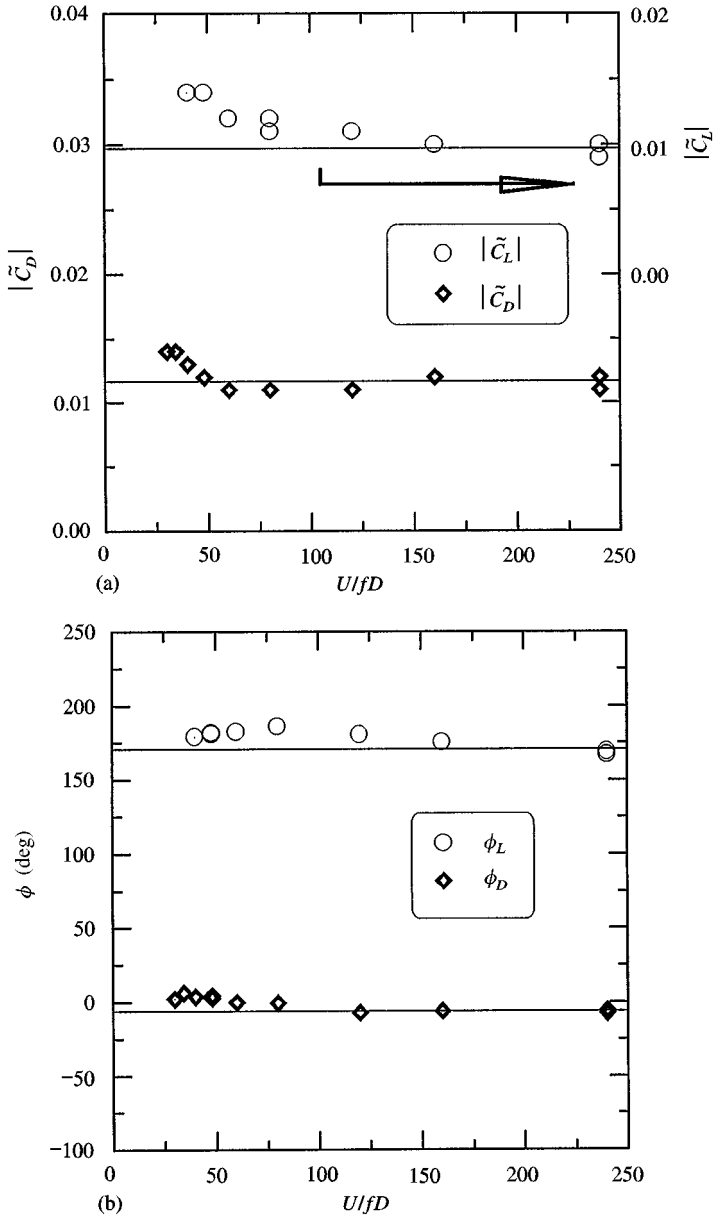

Figure 15. The fluidelastic force coefficients, $\tilde{C}_D$ and $\tilde{C}_L$, on the stationary, downstream cylinder for Case 7 ($L/D = 1{\cdot}84$, $T/D = -0{\cdot}93$, $A/D = 0{\cdot}043$) at $\mathrm{Re} = 7{\cdot}1 \times 10^4$ as functions of the reduced flow velocity, U/fD: (a) magnitudes, $|\tilde{C}_D|$ and $|\tilde{C}_L|$; (b) phase angles of the fluid forces on the downstream cylinder with respect to the displacement of the upstream one, ϕ_D and ϕ_L. The horizontal lines denote the asymptotes which are defined as the averages of the three data-points at the largest U/fD.

the weak proximity interference region, i.e., the instrumented cylinder is oscillating upstream, where the lift force acting on it is very small, and the drag is affected by the presence of the downstream cylinder. The values for $|\tilde{C}_D|$ and $|\tilde{C}_L|$, and the corresponding phase

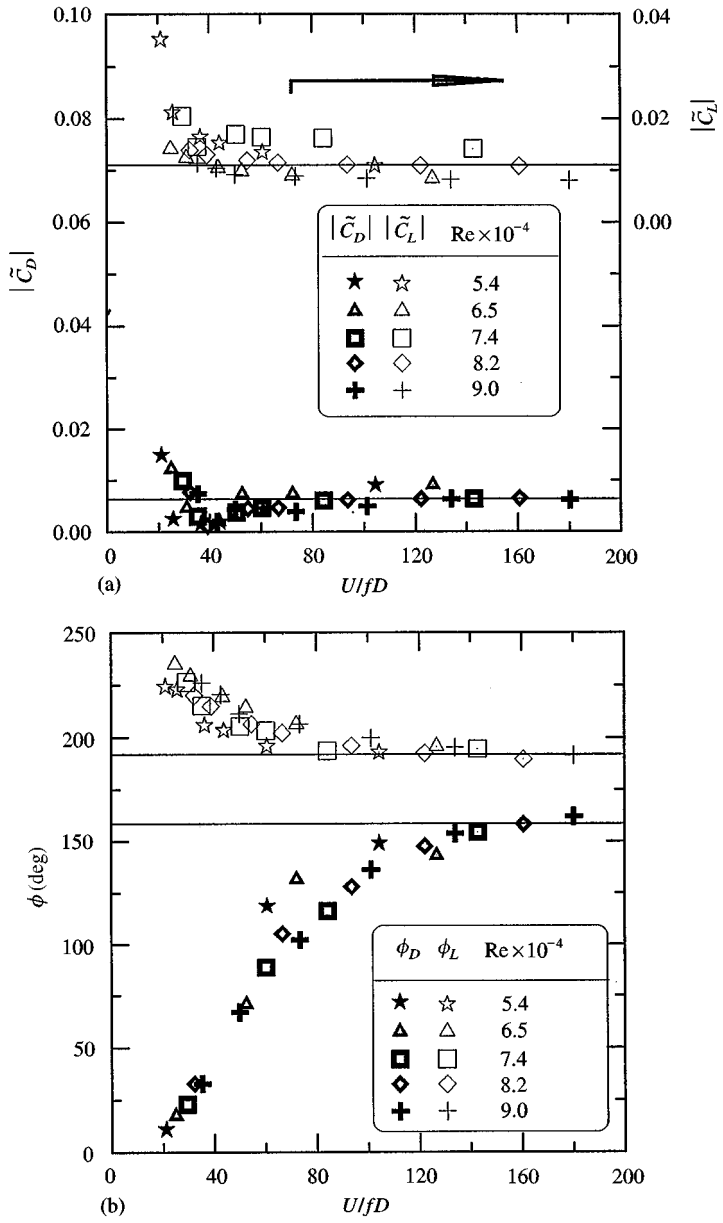

Figure 16. The fluidelastic force coefficients, $\tilde{C}_D$ and $\tilde{C}_L$, on the oscillating, upstream cylinder for Case 6 ($L/D = 2{\cdot}00$, $T/D = 0{\cdot}92$, $A/D = 0{\cdot}047$) as functions of the reduced flow velocity, U/fD: (a) magnitudes, $|\tilde{C}_D|$ and $|\tilde{C}_L|$; (b) phase angles of the fluid forces with respect to the cylinder displacement, ϕ_D and ϕ_L. The horizontal lines denote the asymptotes which are defined as the averages of the three data-points at the largest U/fD.

angles, ϕ_D and ϕ_L, are plotted as functions of U/fD in Figure 16(a, b). Over the range of conditions considered, the effects of Re are small. The values of $|\tilde{C}_D|$, $|\tilde{C}_L|$, ϕ_D and ϕ_L remain roughly constant for U/fD larger than about 100. The phase angle in the drag direction, ϕ_D, deviates from the steady value at relatively large U/fD. It is noticed that $|\tilde{C}_D|$

TABLE 3
Organization of the cases according to the complexity of fluidielastic force results

Flow complexity	Case	Spacing	Flow region	Critical U/fD
Severe	10	($L/D = 1{\cdot}50$, $T/D = 0{\cdot}20$)	Inner lift peak, sensitive	> 250
Severe	8	($L/D = 2{\cdot}00$, $T/D = 0{\cdot}17$)	Inner lift peak, sensitive	$\gg 15$[†]
Severe	9	($L/D = 2{\cdot}00$, $T/D = 0{\cdot}10$)	Inner lift peak, sensitive	140
Moderate	5	($L/D = 2{\cdot}94$, $T/D = -0{\cdot}50$)	in the boundary of the inner lift peak	125
Mild	4	($L/D = 3{\cdot}97$, $T/D = -1{\cdot}05$)	Outside the outer lift peak	60
Mild	3	($L/D = 4{\cdot}00$, $T/D = 1{\cdot}00$)	Outside the outer lift peak	$15 \sim 132$
Mild	2	($L/D = 4{\cdot}00$, $T/D = 1{\cdot}03$)	Outside the outer lift peak	60
Mild	7	($L/D = 1{\cdot}84$, $T/D = -0{\cdot}93$)	Outside the inner lift peak	50
Mild	1	($L/D = 5{\cdot}00$, $T/D = 0{\cdot}50$)	$5D$ downstream, away from the sensitive flow regions	< 44
Special	6	($L/D = 2{\cdot}00$, $T/D = 0{\cdot}92$)	Proximity region, oscillation and measurement on upstream cylinder	100

[†] Only tested at $U/fD = 15$.

in this case is substantially smaller than in other cases; hence, errors in determining $|\tilde{C}_D|$ and ϕ_D (especially ϕ_D) can be expected to be relatively large. Although the general trends in Figure 16 are reliable, disregarding ϕ_D would lower the critical reduced flow velocity, at which the dynamic values start to depart from the asymptotic values, from roughly 100 to 60. The severe deviation of ϕ_D from its asymptotic value with decreasing U/fD may be one of the unique characteristics of the fluidelastic forces of an oscillating cylinder located upstream of another cylinder in the proximity interference region.

8.3. ORGANIZING THE CASES

The static force coefficient map furnished by Zdravkovich (1987), Figure 1, can assist in the organization of the ten cases tested in this study. In general, when the cylinder under consideration is outside the sensitive flow regions, the dynamic force coefficients remain roughly unchanged with respect to changes in U/fD, for U/fD larger than approximately 60. The critical reduced flow velocity, below which the dynamic force coefficients ($|\tilde{C}_D|$, $|\tilde{C}_L|$, ϕ_D or ϕ_L) depart rapidly from the corresponding asymptotic values, increases significantly as the cylinder approaches the complex flow regions; specifically, the inner and outer lift peak regions. Thus, it is possible to arrange the different cases according to the complexity of the flow surrounding the cylinder. Such an attempt, where nine of the ten cases tested are organized in order of decreasing flow complexity, is given in Table 3. Note that Case 6 is considered to be unique (proximity interference) in this set of results, and hence has not been included in this classification.

9. CONCLUSIONS

The fluidelastic forces for two staggered circular cylinders of equal diameter in air cross-flow have been measured in a low-speed wind tunnel, using both pressure distribution and force measurement techniques. One cylinder was forced to oscillate harmonically in the

transverse direction, while measuring the pressure distribution or forces on the same or the stationary cylinder. The forcing frequency and free-stream velocity were varied from 1 to 16 Hz and from 10 to 35 m/s, respectively, giving $4 \times 10^4 \leq \mathrm{Re} \leq 2 \times 10^5$ and $15 \leq U/fD \leq 300$. Ten different geometrical arrangements have been considered, concentrating mostly in the vicinity of the inner and outer lift peaks, along with one case in the weak proximity interference region. The pressure distribution measurements were made with $A/D = 0{\cdot}17$, and they were processed in the time domain. On the other hand, direct force measurements were made with $A/D = 0{\cdot}047$ or $0{\cdot}043$, and the results were processed in the frequency domain.

Processing the pressure measurement in the time domain gives the actual path traced by the dynamic forces as the cylinder oscillates. However, pressure distribution measurements are very tedious, and the data reduction process in the time domain is prone to noise interference. Data processing is simplified significantly when the force signals are processed in the frequency domain, where the required signal can be isolated from both noise and other flow-related signals. However, processing the signals in the frequency domain eliminates the possibility of determining the actual force–displacement loop; instead, only the mean elliptical paths can be deduced.

A reasonably comprehensive set of experimental data on fluidelastic forces for two staggered circular cylinders of equal diameter in air cross-flow has been documented. At large reduced flow velocity, U/fD, the dynamic results approach the asymptotic results. The corresponding force–displacement plot is a linear path with very little hysteresis. Below a critical reduced flow velocity, the dynamic forces depart from the corresponding asymptotic values rapidly with decreasing reduced flow velocity. The departure is portrayed in terms of diverging magnitude and phase angle of the fluidelastic forces in the frequency domain. In the time domain, this departure is shown as a significant increase in the hysteresis of the force–displacement loops, sometimes with changes in the shape of the loops.

The value of the critical reduced flow velocity at which the fluidelastic forces depart from the asymptotic values is very sensitive to the underlying flow around the cylinder. For small-amplitude oscillation, the flow characteristics may be inferred from the static force coefficient map furnished by Zdravkovich (1987). Away from the sensitive flow regions, such as the inner and outer lift peaks, the critical reduced flow velocity can be as low as 50. In the sensitive flow region (i.e., close to the centre of the inner lift peak region), however, this critical reduced flow velocity can be larger than 250.

A number of unresolved issues remain. One is the strong dependence, in some cases, of the values of $\tilde{C}_D$ and $\tilde{C}_L$ on whether it is the upstream or the downstream cylinder that is oscillated (while measuring the force coefficients on the downstream one). Also, despite the general agreement on the critical U/fD discussed in the preceding paragraph, the degree of divergence of $\tilde{C}_D$ and $\tilde{C}_L$ from their asymptotes as U/fD is reduced varies widely from one case to another; the reason for that also seems unclear. This and other issues of this type may be resolved with the aid of flow visualization studies.

ACKNOWLEDGEMENTS

The authors gratefully acknowledge the financial support of the Natural Sciences and Engineering Research Council of Canada and Le Fonds FCAR of Québec. The authors are indebted to E. A. Pinnell and P. W. Sychterz for conducting and analysing the pressure-based measurements.

References

Achenbach, E. 1968 Distribution of local pressure and skin friction around a circular cylinder in cross-flow up to $\mathrm{Re} = 5 \times 10^6$. *Journal of Fluid Mechanics* **34,** 625–639.

Allen, J. H. & Vincenti, W. G. 1994 Wall interference in a two-dimensional flow wind tunnel, with consideration of the effect of compressibility. National Advisory Committee for Aeronautics Report 782.

Batham, J. P. 1973 Pressure distributions on circular cylinders at critical Reynolds numbers. *Journal of Fluid Mechanics* **57,** 209–228.

Bearman, P. W. & Luo, S. C. 1988 Investigation of the aerodynamic instability of a square-section cylinder by forced oscillation. *Journal of Fluids and Structures* **2,** 161–176.

Bishop, R. E. D. & Hassan, A. Y. 1964 The lift and drag forces on a circular cylinder oscillating in a flowing fluid. *Proceedings of the Royal Society (London)* Series A, **277,** 51–75.

Blevins, R. D. 1977 *Flow-Induced Vibration*. New York: Van Nostrand Publishing. (Second edition, New York: Van Nostrand Publishing, 1990.)

Chen, S. S. 1987*a* *Flow-Induced Vibration of Circular Cylindrical Structures*. Washington: Hemisphere Publishing.

Chen, S. S. 1987*b* A general theory for dynamic instability of tube arrays in crossflow. *Journal of Fluids and Structures* **1,** 35–53.

Chen, S. S. 1989 Some issues concerning fluidelastic instability of a group of cylinders in crossflow. *ASME Journal of Pressure Vessel Technology* **111,** 507–518.

Chen, S. S., Zhu, S. & Jendrzejczyk, J. A. 1994 Fluid damping and fluid stiffness of a tube row in crossflow. In *Flow-Induced Vibration-1994* (eds M. K. Au-Yang & K. Fujita), PVP-Vol. 273, pp. 15-31. New York: ASME.

Fage, A. & Falkner, V. M. 1931 The flow around a circular cylinder. Aeronautical Research Council Reports and Memoranda No. 1369.

Fung, T. C. 1960 Fluctuating lift and drag acting on a cylinder in a flow at supercritical Reynolds numbers. *Journal of the Aerospace Sciences* **27,** 801–814.

Goyder, H. G. D. & Teh, C. E. 1984 Measurement of the destabilising forces on a vibrating tube in a fluid cross flow. *Proceedings of ASME Symposium on Flow-Induced Vibration and Noise*, Vol. 2 (eds M. P. Païdoussis, M. K. Au-Yang & S. S. Chen), pp. 151–163. New York: ASME.

Griffin, O. M. 1980 OTEC cold water pipe design for problems caused by vortex-excited oscillations. NRL Memorandum Report 4157, Naval Research Laboratory, Washington, D.C., U.S.A.

Halfman, R. L. 1952 Experimental aerodynamic derivatives of a sinusoidally oscillating airfoil in two-dimensional flow. National Advisory Committee for Aeronautics Report 1108.

Holman, J. P. &. Gajda, W. J. Jr 1989 *Experimental Methods for Engineers*, 5th edition. New York: McGraw-Hill.

Luo, S. C. & Bearman, P. W. 1990 Predictions of fluctuating lift on a transversely oscillating square-section cylinder. *Journal of Fluids and Structures* **4,** 219–228.

Mair, W. A. & Maull, D. J. 1971 Aerodynamic behaviour of bodies in the wakes of other bodies. *Philosophical Transactions of the Royal Society (London)* A, **269,** 425–437.

Norberg, C. & Sundén, B. 1987 Turbulence and Reynolds number effects on the flow and fluid forces on a single cylinder in cross flow. *Journal of Fluids and Structures* **1,** 337–358.

Ohya, Y. O., Okajima, A. & Hayashi, M. 1989 Wake interference and vortex shedding. *Encyclopedia of Fluid Mechanics — Aerodynamics and Compressible Flow* **8,** 322–389.

Otsuki, Y., Washizu, K., Tomizawa, H. &. Ohya, A. 1974 A note on the aeroelastic instability of a prismatic bar with square section. *Journal of Sound and Vibration* **34,** 233–248.

Païdoussis, M. P. 1980 Flow-induced vibrations in nuclear reactors and heat exchangers: practical experiences and state of knowledge. In *Practical Experiences with Flow-Induced Vibrations* (eds E. Naudascher & D. Rockwell), pp. 1–81. Berlin: Springer.

Païdoussis, M. P. 1981 Fluidelastic vibration of cylinder arrays in axial and cross-flow: state of the art. *Journal of Sound and Vibration* **76,** 329–360.

Païdoussis, M. P. 1983 A review of the flow-induced vibrations in reactors and reactor components. *Nuclear Engineering and Design* **74,** 31–60.

Païdoussis, M. P. 1993 Some curiosity-driven research in fluid structure interactions and its current applications. Calvin Rice lecture. *ASME Journal of Pressure Vessel Technology* **115,** 2–14.

PAÏDOUSSIS, M. P., PRICE, S. J. & WANG, D. J. 1994 An experimental study of the applicability of the quasi-steady assumption for staggered cylinders in cross-flow. In *Flow-Induced Vibration–1994* (eds M. K. Au-Yang & K. Fujita), PVP-Vol. 273, pp. 157–172. New York: ASME.

PARKINSON, G. V. 1989 Phenomena and modelling of flow-induced vibrations of bluff bodies. *Progress in Aerospace Science* **26,** 169–224.

PINNELL, E. A. 1987 An investigation of the quasi-steady assumption in single and staggered cylinder configurations subjected to air crossflow. Master's Thesis, Faculty of Engineering, McGill University.

PRICE, S. J. 1976 The origin and nature of the lift force on the leeward of two bluff bodies. *Aeronautical Quarterly* **26,** 154–168.

PRICE, S. J. 1995 A review of theoretical models for fluidelastic instability of cylinder arrays in cross-flow. *Journal of Fluids and Structures* **9,** 463–518.

PRICE, S. J. & PAÏDOUSSIS, M. P. 1984 The aerodynamic forces acting on groups of two and three circular cylinders when subject to a cross-flow. *Journal of Wind Engineering and Industrial Aerodynamics* **17,** 329–347.

PRICE, S. J., PAÏDOUSSIS, M. P. & SYCHTERZ, P. W. 1988 An experimental investigation of the quasi-steady assumption for bluff bodies in cross-flow. In *Proceedings ASME/CSME/IMechE/IAHR International Symposium on Flow-Induced Vibration and Noise*, Vol. 1 (eds M. P. Païdoussis, O. M. Griffin & C. Dalton), pp. 91–111. New York: ASME.

ROSHKO, A. 1961 Experiments on the flow past a circular cylinder at very high Reynolds number. *Journal of Fluid Mechanics* **10,** 345–356.

SARPKAYA, T. 1978 Fluid forces on oscillating cylinders. *ASCE Journal of the Waterway, Port, Coastal and Ocean Engineering Division* **104,** 275–290.

SHIN, Y. S. & WAMBSGANSS, M. W. 1977 Flow-induced vibration in LMFBR steam generators: a state-of-the -art review. *Nuclear Engineering and Design* **40,** 235–284.

SYCHTERZ, P. W. 1990 An investigation of the quasi-static assumption for a pair of staggered cylinders in cross-flow. Master's Thesis, Faculty of Engineering, McGill University.

TANAKA, H. & TAKAHARA, S. 1980 Unsteady fluid dynamic force on tube bundle and its dynamic effect on vibration. In *Flow-Induced Vibration of Power Plant Components* (ed M. K. Au-Yang), pp. 79–92. New York: ASME.

TANAKA, H. & TAKAHARA, S. 1981 Fluidelastic vibration of tube array in cross-flow. *Journal of Sound and Vibration* **77,** 19–37.

TANIDA, Y., OKAJIMA, A. & WATANABE, Y. 1973 Stability of a circular cylinder oscillating in uniform flow or in a wake. *Journal of Fluid Mechanics* **61,** 769–784.

TING, D. S-K. WANG, D. J., PRICE, S. J. & PAÏDOUSSIS, M. P. 1997 The applicability of the quasi-steady assumption for two staggered circular cylinders in cross-flow. In *Proceedings 4th Int'l Symposium on Fluid-Structure Interactions, Aeroelasticity, Flow-Induced Vibration and Noise* (eds. M. P. Païdoussis *et al.*) Vol. 1, AD-Vol. 53-1, pp. 159–168. New York : ASME.

WANG, D. J. 1995 An experimental study of the applicability of the quasi-steady assumption for staggered cylinders in cross-flow. Ph.D. Thesis, Faculty of Engineering, McGill University.

WASHIZU, K., OHYA, A., OTSUKI, Y. & FUJII, K. 1978 Aeroelastic instability of rectangular cylinders in a heaving mode. *Journal of Sound and Vibration* **59,** 195–210.

WEST, G. S. & APELT, C. J. 1982 The effect of tunnel blockage and aspect ratio on the mean flow past a circular cylinder with Reynolds number between 10^4 and 10^5. *Journal of Fluid Mechanics* **114,** 361–377.

ZDRAVKOVICH, M. M. 1977 Review of flow interference between two circular cylinders in various arrangements. *ASME Journal of Fluids Engneering* **99,** 618–631.

ZDRAVKOVICH, M. M. 1987 The effects of interference between circular cylinders in cross flow. *Journal of Fluids and Structures* **1,** 239–262.

ZDRAVKOVICH, M. M. & PRIDDEN, D. L. 1977 Interference between two circular cylinders; series of unexpected discontinuities. *Journal of Industrial Aerodynamics* **2,** 255–270.

APPENDIX: NOMENCLATURE

A	amplitude of the transverse oscillation
C_D	drag coefficient; positive in the $+X$ direction (see Figure 2)

C_{Do}	static drag coefficient when the "oscillating" cylinder is stationary at its mean lift position; positive in the $+X$ direction (see Figure 2)
$\bar{C}_D$	steady drag coefficient obtained from measurements while one of the cylinders is oscillating; positive in the $+X$ direction (see Figure 2)
$\tilde{C}_D$	dynamic drag coefficient; positive in the $+X$ direction (see Figure 2)
C_L	lift coefficient; positive in the $+Y$ direction (see Figure 2)
C_{Lo}	static lift coefficient when the "oscillating" cylinder is stationary at its mean lift position; positive in the $+Y$ direction (see Figure 2)
$\bar{C}_L$	steady lift coefficient obtained from measurements while one of the cylinders is oscillating; positive in the $+Y$ direction (see Figure 2)
$\tilde{C}_L$	dynamic lift coefficient; positive in the $+Y$ direction (see Figure 2)
D	diameter of the cylinders
f	forcing frequency
F	force
l	length of the cylinder in the wind tunnel test-section
L	streamwise centre-to-centre distance between the two cylinders (see Figure 2)
P	pitch between the centres of the two cylinders (see Figure 2)
q	dynamic pressure
Re	Reynolds number based on the diameter of the cylinder ($= UD/\nu$)
t	time
T	transverse centre-to-centre distance between the two cylinders (see Figure 2)
U	free-stream velocity
W_r	response parameter $[=(1 + 2A/D)(fD/US)]$
y	displacement of the oscillating cylinder
ν	dynamic viscosity
ρ	density of the fluid
ϕ_D	phase angle of $\tilde{C}_D$ with respect to cylinder displacement, $y(t)$
ϕ_L	phase angle of $\tilde{C}_L$ with respect to cylinder displacement, $y(t)$